Creation of Optical Cat and GKP States Using Shaped Free Electrons

Raphael Dahan,[1,†] Gefen Baranes,[2,†] Alexey Gorlach,[1] Ron Ruimy,[1] Nicholas Rivera,[2,3] and Ido Kaminer[1,*]
[1]Technion—Israel Institute of Technology, Haifa 32000, Israel
[2]Massachusetts Institute of Technology, Cambridge, Massachusetts 02139, USA
[3]Harvard University, Cambridge, Massachusetts 02138, USA

(Received 17 June 2022; revised 18 April 2023; accepted 24 April 2023; published 6 July 2023)

Cat states and Gottesman-Kitaev-Preskill (GKP) states play a key role in quantum computation and communication with continuous variables. The creation of such states relies on strong nonlinear light-matter interactions, which are widely available in microwave frequencies as in circuit quantum electrodynamics platforms. However, strong nonlinearities are hard to come by in optical frequencies, severely limiting the development and applications of quantum-information science with continuous variable in the optical range. Here we propose using the strong interaction of free electrons with light to implement the desired nonlinear mechanism, showing its implication by creating optical cat and GKP states. The key to our finding is identifying conditions on the electron for which its interaction mimics the conditional displacement quantum gate. The strong interactions can be realized by phase matching of free electrons with photonic structures such as optical waveguides and photonic crystals in an ultrafast transmission electron microscope (UTEM). Our approach enables the generation of optical GKP states with above 10 dB squeezing and fidelities above 90% at postselection probability of 10%, even reaching $> 30\%$ using an initially squeezed-vacuum state. We analyze the different factors that affect the fidelity, such as electron dispersion, inhomogeneity, nonideal interaction, and limited detection efficiency. Furthermore, the free-electron interaction allows two qubit gates between a pair of GKP states, which can entangle them into a GKP Bell state. We present a roadmap for realizing such experiments in a UTEM. Since electrons can interact resonantly with light across the electromagnetic spectrum, our approach could apply for a generation of cat and GKP states also in other platforms of free-electron radiation, from klystrons to free-electron lasers.

DOI: 10.1103/PhysRevX.13.031001 Subject Areas: Photonics, Quantum Information

I. INTRODUCTION

The fundamental interaction between an electromagnetic field and free electrons forms the basis of electrodynamics. The radiation emitted by the electrons can span a wide spectral range, extending from radio waves all the way up to x rays, as in cyclotron radiation, traveling-wave tubes, the Cherenkov effect, x-ray tubes, and free-electron lasers [1]. The classical properties of radiation, such as intensity and frequency, can be controlled by the classical electron characteristics such as its acceleration along a trajectory. Control of such electron characteristics has been the cornerstone of free-electron radiation technologies, using either static electromagnetic fields as in synchrotron radiation [2–4] or oscillating fields as in Compton scattering [2,5,6].

Importantly, ever since the work of Glauber and other luminaries [7–9], it is widely appreciated that the full nature of light goes far beyond its classical characteristics. There are also quantum degrees of freedom, such as entanglement and the degrees of coherence. In general, realizing full control of the quantum state of light is a long-standing open problem in quantum optics. The state of light can hold quantum information in its harmonic-oscillator Hilbert space serving as a so-called continuous variable (CV) [10], in contrast with more conventional two-level (qubit) systems that serve as discrete variables. Substantial efforts are invested in an efficient generation of quantum-light CV states that could enable fault-tolerant quantum computing [10–13] and better quantum-key-distribution protocols [14–16].

Prominent examples of desirable quantum states for use in CV quantum systems are the Gottesman-Kitaev-Preskill (GKP) states [11]. These states have been specifically designed to exhibit robustness against displacement errors and photon loss, which are the primary sources of noise in optical systems. Over the years, a diverse range of approaches have been proposed for GKP-state preparation, including active stabilization protocols [11,17,18], post-selection methods [19–28], and passive error correction

*kaminer@technion.ac.il
†R. D. and G. B. contributed equally to this work.

through Hamiltonian engineering [29,30]. So far, GKP states were demonstrated in the microwave frequency range in platforms of circuit quantum electrodynamics and ion traps [17,18,23], recently showing improved quantum coherence time beyond that of the physical quantum components [31]. More generally, all the states that enable universal quantum computation with CVs are part of the so-called non-Gaussian states [10,32] (states whose Wigner quasiprobability distribution is not a Gaussian function). Unfortunately, the desired non-Gaussian states such as GKP states are yet to be demonstrated in the optical range, due to the generally weak nature of optical nonlinearities [24,33].

Current theoretical proposals for the generation of optical GKP states rely on optical Kerr effects [20,27], cavity QED [28], homodyne measurements of cat states [22,34], or measurement-based schemes that require photon-number-resolving detection [24–26]. However, all these optical schemes are currently limited to the generation of just a few photons with low fidelities, because they rely on the intrinsically weak optical nonlinearities or on low postselection probabilities. This is why no optical experiment so far has reached a non-Gaussian state of sufficient photon number and sufficient squeezing to be usable for CV quantum computation. Despite the difficulties in creating optical GKP states, there is an ongoing intense search for new mechanisms to generate them and unlock their prospects for photonic quantum technologies.

Here we propose to exploit interactions between free electrons and photonic structures to generate GKP states and other non-Gaussian states that can facilitate fault-tolerant quantum computing. Our approach provides control over the quantum state of free-electron radiation by preshaping the electron wave function before its radiation emission and postselecting the electron energy afterward. Specifically, we propose energy-comb electrons as a natural basis for controlling the photonic states created via the interaction. A free-electron comb is a superposition of electron energy eigenstates in which the energies form an evenly spaced ladder, analogous to an optical-frequency comb of evenly spaced frequencies. We show how cat states and multicomponent cat states can be heralded by energy postselection of comb electrons. Consequent interactions of multiple comb electrons with appropriate postselections create more complex photonic states such as the GKP state. We find that the postselection probability to produce a GKP state of 10 dB squeezing is $>10\%$, on par with current leading theoretical proposals for the creation of optical GKP states [20,22,24–28,34]. We further present more advanced schemes that increase the probability to $>30\%$ by "seeding" the electron radiation process with a squeezed vacuum state that can be generated using spontaneous parametric processes [35]. We identify the shaped-electron interaction with light as a conditional displacement of the optical state (conditioned on the electron state). The conditional displacement together with feed forward allow for error-correction protocols and universal control of the harmonic-oscillator quantum state [36]. Finally, we demonstrate how the interactions with comb electrons can apply gates on two GKP qubits, for example, entangling two photonic modes into a GKP Bell state—an important step toward the vision of GKP cluster states for fault-tolerant quantum computation.

Earlier papers suggested [37,38] and demonstrated [39] that postselection on shaped free electrons alters the properties of their emission. In a different approach, without preshaping, free electrons were proposed as single-photon emitters [40] and recently utilized in an experiment to create quantum-correlated electron-photon pairs [41]. Moreover, photon addition or subtraction through free-electron postselection was proposed for generating Fock states, photon-added coherent states, or photon-subtracted thermal states [42]. Other recent works unveiled the dependence of the second-order coherence of the emitted light on the electron's wave-function duration and shape [43–46]. A significant research effort over the past decade explored the shaping of the single-electron wave function in the longitudinal [47–52] and transverse [51–63] directions. Most importantly for our approach, time-energy shaping of a free-electron wave function was demonstrated by ultrafast transmission electron microscopy (UTEM) [47,48]. Such temporal shaping has shown in recent years the creation of coherent free-electron attosecond bunches [49] and free-electron energy combs [64–66]. These advances show the feasibility of the concept we suggest here.

II. RESULTS

A. Creation of quantum state of light using coherent free-electron combs

Before presenting the theory and main results, we start by introducing the key novel element of our proposal for generating optical cat and GKP states: the interaction between a quantized mode of light and a free electron. The radiation by a free electron by and large has been considered to be completely classical, and this classicality underlies much research in electron-based light sources even today [67,68]. Such a "classicality" has long been justified from a quantum-mechanical perspective by equating the electron to a classical current [8], which generates a coherent state, the most classical state of light. However, the true quantum nature of the electron is that of a free quantum particle with a continuous spectrum that can undergo single-photon-emitting transitions at nearly arbitrary frequencies. By understanding the electron along these lines, treating the electron-light interaction in a fully quantized theory, many new and exotic quantum effects emerge. While one might expect the quantum electron-light interaction to be similar to the interaction of two-level systems with light captured by the Jaynes-Cummings and

Rabi model, many new effects emerge due to the continuous spectrum of the electron [42]. Many of these new effects arise from the fact that the electron can emit and absorb many photons, as has been extensively experimentally tested in recent years. Moreover, many new effects also emerge by shaping the electron wave function via electron optics, creating complex superpositions of motional states.

That all said, in many cases, free electrons are "natural" generators of coherent states of light. This capability of electrons, in addition with the ability to generate complex superposition states, as we now show, leads to the ability to create superpositions of macroscopically populated coherent states, i.e., Schrödinger cat states, also enabling the possibility of generating GKP states. The main technical result of this work is that free-electron-light interactions implement conditional displacements, which, beyond the application proposed here, should lead to many new developments in the physics of free-electron radiation.

The process we propose for creating desired non-Gaussian quantum states consists of three building blocks (Fig. 1): (a) generation of shaped electrons (i.e., comb electrons), (b) efficient free-electron-photon interaction (in the strong-coupling regime), and (c) electron energy postselection. We assume a highly paraxial electron with energy much higher than that of the photon with which it interacts, yet energy uncertainty smaller than the photon energy. This condition is frequently realized in transmission and scanning electron microscopes, as exemplified by different experiments in photon-induced near-field electron microscopy (PINEM) [47–52,61,63–66,69–72], and explained theoretically in Refs. [73,74].

Using a quantum-optical framework, the interaction between a free electron and an optical mode is captured by the scattering matrix (as first proposed in Refs. [78,79] and demonstrated experimentally in Ref. [70])

$$S = \exp[g_{\mathrm{Q}} b a^{\dagger} - g_{\mathrm{Q}}^{*} b^{\dagger} a], \tag{1}$$

where a, $a^{\dagger}$ are the annihilation and creation operators for the photonic mode; b, $b^{\dagger}$ (satisfying $bb^{\dagger} = b^{\dagger}b = 1$, like the quantum rotor [80]) are operators describing an electron translation in energy, which correspond to the emission or absorption of a single photon.

Equation (1) shows that the interaction between an electron and an optical mode is approximately analogous to the beam-splitter interaction of two optical modes [8]. However, a key difference between Eq. (1) and a beam-splitter interaction is that the electron ladder operators commute ($[b, b^{\dagger}] = 0$) in contrast with the photonic operators that do not commute ($[a, a^{\dagger}] = 1$). This contrast makes a big impact on the central features arising from electron interactions, creating both fundamental and technical differences relative to other schemes in the field (elaborated in a dedicated section below).

A general electron wave function is described as a superposition of monoenergetic states $|n\rangle_e = |E_0 + n\hbar\omega\rangle_e$, each describing an electron shifted by a multiple of the photon energy $n\hbar\omega$. We use the term "monoenergetic" for an electron state with an energy width smaller than the photon energy $\hbar\omega$, which is a standard condition satisfied in PINEM experiments (e.g., Refs. [47–52,61,63–66,69–72]). The condition to consider the electron as occupying such a discrete ladder of energy states is that the electron interacts predominantly with a single optical mode of frequency ω. In conventional PINEM experiments that probe stimulated interactions, this condition is ensured by the pump-laser linewidth, which creates a narrow-bandwidth excitation. In the spontaneous (nonpumped) case we consider here, the condition to consider the electron as on a discrete ladder is that it predominantly emits into a single optical mode. Using this notation, the electron translation operators satisfy $b^{\dagger}|n\rangle_e = |n+1\rangle_e$, $b|n\rangle_e = |n-1\rangle_e$. We choose the state $|0\rangle_e$ as the initial electron state before it is shaped into a comb.

The coupling constant g_{Q} is a dimensionless complex parameter that describes the interaction strength and the phase between the optical mode and the free electron. g_{Q} is defined using the electric field E of the optical mode normalized to the amplitude of a single photon, with v being the electron velocity and $r_{\perp}$ being its transverse location: $g_{\mathrm{Q}} = (q_e/\hbar\omega)\int E_z(r_{\perp}, z) e^{-i\omega z/v} dz$ [78]. Equivalently, g_{Q} can also be derived from the Green's function of the optical structure [81]: $|g_{\mathrm{Q}}|^2 = (q_e^2 \mu_0/\pi\hbar)\int \mathrm{Im}G_{zz}(r_{\perp}, z; r_{\perp}, z'; \omega) e^{-i\omega(z-z')/v} dz dz'$. In general, g_Q is a function of (x, y) in the transverse direction. It can be precisely controlled by the distance of the electron beam from the evanescent part of the optical mode.

The free-electron wave function can be shaped in the time domain, i.e., undergo a temporal modulation induced by the interaction as in PINEM [47–52,61,63–66,69–72] or the pondermotive interaction [82–84]. In this paper, we consider electrons shaped as energy combs with a periodicity of multiple photon energy $N\hbar\omega$ and equal phases (see Supplemental Material [85] Sec. I). Such an ideal electron comb can be approximated by shaping a monoenergetic electron using multiple frequencies [75] or multiple interaction stages [76]. The next section shows that these combs can be used for heralding different cat states, under certain energy postselection conditions.

B. Creation of N-component cat states

Let us focus on the creation of multicomponent cat states [9] (known as multilegged cat states), which can be described as $|\mathrm{cat}_N^k\rangle_{\mathrm{ph}} \propto \sum_{m=0}^{N-1} \exp(-2\pi i k m/N) |\exp(2\pi i m/N)\alpha\rangle_{\mathrm{ph}}$, where $|\alpha\rangle_{\mathrm{ph}}$ describes a coherent state. To create the N-component cat state, we prepare a comb electron $|\mathrm{comb}_N^0\rangle_e \propto \sum_{n=-\infty}^{\infty} |E_0 + nN\hbar\omega\rangle_e$ with an energy spacing of $N\hbar\omega$

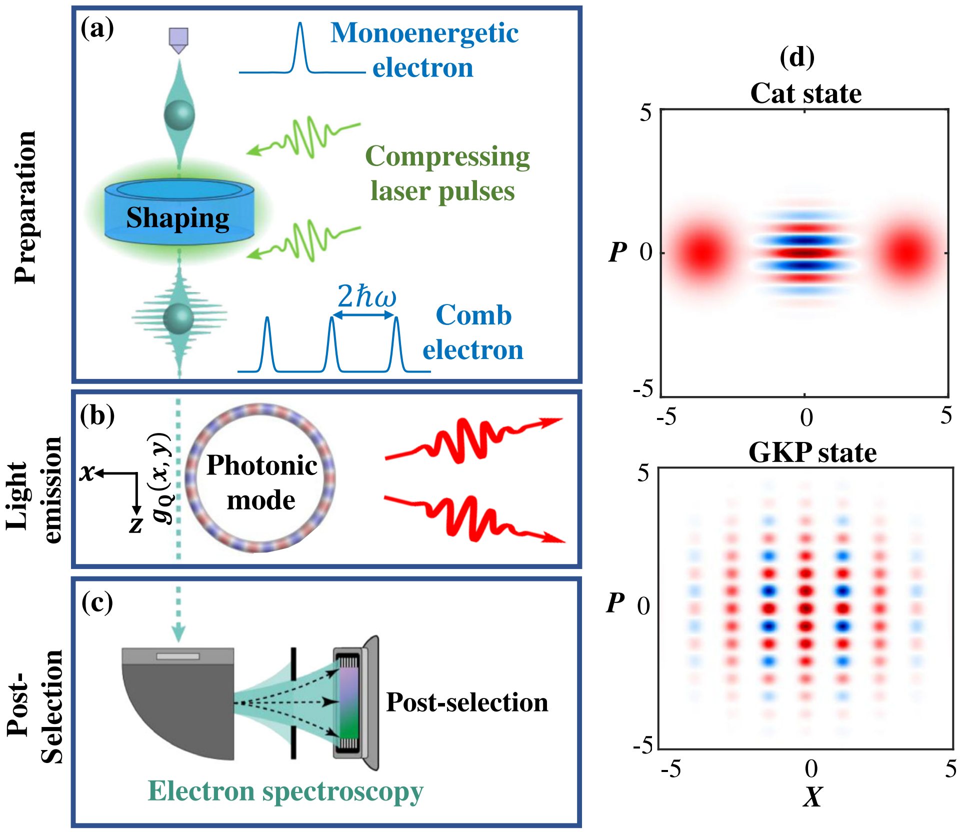

FIG. 1. Generating optical cat and GKP states using free electrons. A scheme of free-electron-based cat- and GKP-state generation divided into three main stages. (a) Preparation stage: A monoenergetic electron is shaped into a comb with an energy spacing of $N\hbar\omega$. The case illustrated here shows $N = 2$. The shaping of free electrons can be implemented using a few harmonics [75] or a few points of interaction [76]. Further preparation of the electron, such as collimation for an extended interaction, can be done with electron lenses and deflectors that are common in transmission electron microscopes. (b) Light-emission stage: The electron then interacts with a photonic structure, emitting photons into an optical mode. The coupling efficiency $g_Q = g_Q(x, y)$ can be tuned by changing the electron-beam transverse location (in xy) relative to the structure. The preferred structures are ones designed to guide light in a waveguide or cavity such that the guided mode is phase matched with the electron, achieving a stronger coupling constant (higher g_Q). (c) Postselection stage: The electron is measured, heralding the generated photonic state. In the case illustrated here, if the measured energy is even ($k = 0$), an even cat state is created $|\alpha\rangle_{\mathrm{ph}} + |-\alpha\rangle_{\mathrm{ph}}$. If the measured energy is odd ($k = 1$), an odd cat state is created $|\alpha\rangle_{\mathrm{ph}} - |-\alpha\rangle_{\mathrm{ph}}$. The measurement can be done via EELS equipped with a fast detector [41,77]. (d) Examples of Wigner functions for the photonic states that can be generated via our scheme: A cat state can be generated using an electron comb and a postselection of its energy. A GKP state can be generated using multiple comb electrons with a specific sequence of postselections as described in Table I. ($g_Q = 4$ and $\sqrt{\pi/2}$ for the top and bottom panels, respectively).

[Fig. 2(a)]. We further define the shifted combs to be $|\mathrm{comb}_N^m\rangle_e = b^{\dagger m}|\mathrm{comb}_N^0\rangle_e$, noting that any $|\mathrm{comb}_N^m\rangle_e$ is invariant under b^N. The infinite comb is an idealized case that can be approximated by a finite comb with Gaussian weights. We consider the effect of the Gaussian comb on the fidelity of the generated photonic state, as described in Supplemental Material [85] Sec. V.

Assuming an initially empty optical mode (vacuum state $|0\rangle_{\mathrm{ph}}$), the joint state of the photonic state and a comb electron is $|\Psi_{\mathrm{in}}\rangle = |\mathrm{comb}_N^0\rangle_e \otimes |0\rangle_{\mathrm{ph}}$. The interaction is described by the scattering matrix S from Eq. (1) that acts on the joint state in the following manner (Supplemental Material [85] Sec. II. 2):

$$|\Psi_{\mathrm{out}}\rangle = S|\Psi_{\mathrm{in}}\rangle = \frac{1}{2}\sum_{k=0}^{N-1} c_N^k|\mathrm{comb}_N^{-k}\rangle_e \otimes |\mathrm{cat}_N^k\rangle_{\mathrm{ph}}, \tag{2}$$

where $|\mathrm{cat}_N^k\rangle_{\mathrm{ph}} = (1/c_N^k)\sum_{m=0}^{N-1} e^{-i2\pi mk/N}|g_Q e^{2im\pi/N}\rangle_{\mathrm{ph}}$ is the kth order of the N-component cat state [9], and c_N^k is a normalization factor that captures the probability of postselecting the kth cat.

After the interaction, we postselect the electron energy to have a certain value $k\hbar\omega$ (modulo $N\hbar\omega$), which heralds the emission of a cat state $|\mathrm{cat}_N^k\rangle_{\mathrm{ph}}$ [Figs. 2(a)–2(f)]. For example, for the case of $N = 2$ (i.e., energy spacing $2\hbar\omega$) and postselection of even or odd electron energies

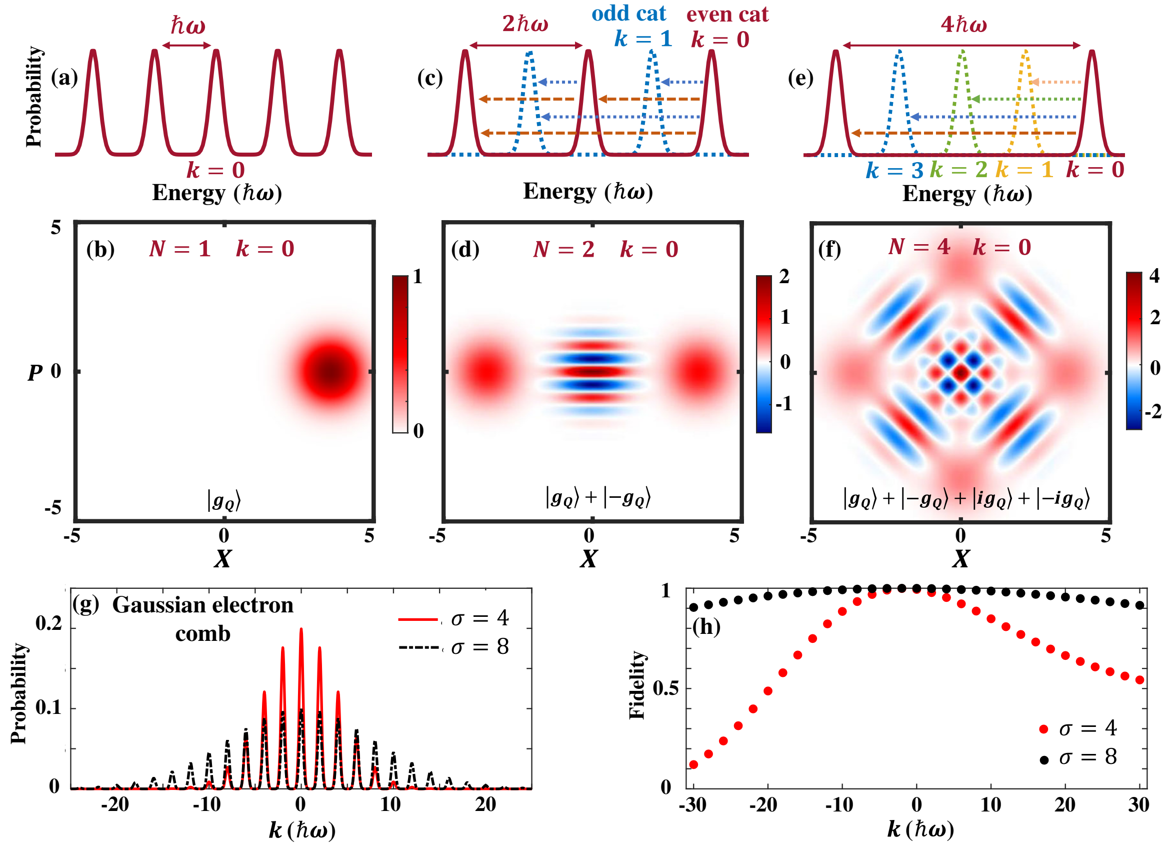

FIG. 2. Characterization of the N-component cat states emitted from a free electron. (a) When a comb electron with an energy spacing of $\hbar\omega$ emits photons of energy $\hbar\omega$, (b) the Wigner function of the photon takes the form of a coherent state. (c) When a comb electron with an energy spacing of $2\hbar\omega$ is postselected for even or odd energies after emitting photons of $\hbar\omega$, (d) the photonic Wigner function takes the form of even or odd cat states. (e) When a comb electron with an energy spacing of $4\hbar\omega$ is postselected after emitting photons of $\hbar\omega$, (f) the photonic Wigner function takes the form of the different four-component cat states. (g) Energy spectra of Gaussian electron combs (energy spacing of $2\hbar\omega$) with a standard deviation of $\sigma = 4$ (red) and $\sigma = 8$ (black) in units of photon energy ($g_Q = \sqrt{\pi/2}$). Such states can be created with high fidelity by three PINEM-type interactions with classical laser light, as described in Ref. [76]. (h) The fidelity of the postselected even cat states after interaction with the Gaussian comb electron. The average fidelity for $\sigma = 4$ is 0.97 and for $\sigma = 8$ is 0.99 (Supplemental Material [85] Sec. V. 2). ($g_Q = 4$ for all panels in this figure. Additional examples with lower g_Q values are provided in the second panels of Figs. 3(a), 4(a), and 4(c) showing the creation of various kitten states.).

($k = 0/1$), the electron radiation takes the form of the even or odd Schrödinger cat state [Figs. 2(c) and 2(d)], i.e., a superposition of two coherent states with opposite signs ($|g_Q\rangle_{\mathrm{ph}}$ and $|-g_Q\rangle_{\mathrm{ph}}$). This process of postselecting even or odd cat states is analogous to a conditional displacement on the photonic mode, where the comb electron plays the role of the conditioning qubit. For any N value, the amplitudes of the cat-state components are proportional to the coupling constant g_Q. The probability to postselect an N-component cat state $|\mathrm{cat}_N^k\rangle_{\mathrm{ph}}$ is given by (Supplemental Material [85] Sec. II.3)

$$P_N^k = \frac{1}{N^2}|c_N^k|^2 = \frac{1}{N^2}\left\| \sum_{m=0}^{N-1} e^{-i2\pi\frac{km}{N}} |e^{i2\pi\frac{m}{N}} g_Q\rangle_{\mathrm{ph}} \right\|^2. \quad (3)$$

C. Creation of GKP states

To create a photonic state in a superposition of many coherent states, we consider multiple comb electrons with $2\hbar\omega$ spacing ($|\mathrm{comb}_2^0\rangle_e$) interacting consequently with an optical mode. For commuting interactions, the electrons can arrive simultaneously as in a multielectron pulse, under the condition of negligible electron-electron repulsion. For now, the optical mode is initiated with a vacuum state before the electron interactions; i.e., the electrons create the desired GKP states through a form of spontaneous emission, rather than a stimulated process.

Consider an interaction with $m + n$ comb electrons, with n of them measured to have an odd energy and m of them measured to have an even energy. For a general initial photonic state $|\psi_i\rangle_{\mathrm{ph}}$, the final photonic state after the interaction is (Supplemental Material [85] Sec. III. 1):

$$
\begin{aligned}
|\psi_f\rangle_{\rm ph} &\propto (D_{g_Q} + D_{-g_Q})^m (D_{g_Q} - D_{-g_Q})^n |\psi_i\rangle_{\rm ph} \\
&\propto \sum_{n_1=0}^{m} \sum_{n_2=0}^{n} \binom{m}{n_1} \binom{n}{n_2} (-1)^{n_2} \\
&\quad \times D_{g_Q(m+n-2n_1-2n_2)} |\psi_i\rangle_{\rm ph},
\end{aligned} \tag{4}
$$

where $D_{g_{\rm Q}} = \exp(g_{\rm Q} a^\dagger - g_{\rm Q}^* a)$ is the displacement operator [8], and $\binom{m}{n_1} = [m!/n_1!(m-n_1)!]$ are the binomial coefficients (similar to grid states proposed by Ref. [22]). Equation (4) provides the possibility to generate different superpositions of coherent states including the squeezed vacuum state.

Superpositions of coherent states that form 2D grid states are possible if considering electron combs with energy spacing higher than $2\hbar\omega$, or by having two different interaction constants (Supplemental Material [85] Sec. III. 2). Among the different 2D grid states, the most attractive are the square- and hexagonal-GKP states [11,86,87]. These GKP states are desired since they enable fault-tolerant universal quantum computation with Gaussian operations [32]. We propose several schemes for the creation of such states (Table I).

The first scheme we present is for the creation of square-GKP states. We choose $4m$ interactions of comb electrons ($|{\rm comb}_2^0\rangle_{\rm e}$ with coupling constant $g_{\rm Q1} = i\sqrt{\pi/8}$. We postselect all of them to have even energies [Fig. 3(a), first row). Then, we introduce m additional interactions of electrons in the state $|{\rm comb}_2^0\rangle_{\rm e}$ with coupling constant $g_{\rm Q2} = \sqrt{\pi/2}$, again postselecting even energies [Fig. 3(a), second row]. Overall, the total number of electrons used in this scheme is $N_e = 5$ m. In order to control the coupling-constant's phase, one can change the phase of the laser used to shape the electron comb or change the region of the mode with

TABLE I. Different protocols for the creation of grid coherent states using electron combs. Rows 1–4 describe different protocols for the creation of approximated square GKP states, with different $g_{\rm Q}$ values. Row 5 shows a protocol for the creation of approximated square GKP states when starting from squeezed vacuum rather than from vacuum. Rows 6–8 show similar protocols for the creation of approximated hexagonal-GKP states. Row 9 shows a protocol for the creation of magic GKP states using comb electrons of $4\hbar\omega$ spacing. The column $g_{\rm Q,max}$ refers to the highest coupling constant used as part of the protocol. $P_{10\ {\rm dB}}$ is the probability to achieve GKP with approximately 10 dB squeezing. N_e is the number of electron interactions required for achieving this squeezing value. The postselection column describes the sequence of postselections necessary to create the state, where E/O stands for even/odd electron energies.

	Initial state	Interaction description	$g_{Q,\max}$	$P_{10\ {\rm dB}}$ (%)	N_e	Post selection	Final state
1	$\|0\rangle_{\rm ph}$	$\sum_{n_1=0}^{2m} \sum_{n_2=0}^{2m} \binom{2m}{n_1}\binom{2m}{n_2} D_{i\sqrt{\frac{\pi}{2}}(n_1-m)} D_{\sqrt{\frac{\pi}{2}}(n_2-m)} \|0\rangle_{\rm ph}$	$\frac{1}{2}\sqrt{\frac{\pi}{2}}$	5	24	EE	$\|0\rangle_{\rm ph}^{\rm GKP}$
2	$\|0\rangle_{\rm ph}$	$\sum_{n_1=0}^{m} \sum_{n_2=0}^{4m} \binom{m}{n_1}\binom{4m}{n_2} D_{\sqrt{\frac{\pi}{2}}(2n_1-m)} D_{i\sqrt{\frac{\pi}{2}}(n_2-2m)} \|0\rangle_{\rm ph}$	$\sqrt{\frac{\pi}{2}}$	9.7	15	EE	$\|0/1\rangle_{\rm ph}^{\rm GKP}$
3	$\|0\rangle_{\rm ph}$	$\sum_{n_1=0}^{m} \sum_{n_2=0}^{m} \binom{m}{n_1}\binom{m}{n_2} D_{\sqrt{\frac{\pi}{2}}(2n_1-m)} D_{i\sqrt{\frac{\pi}{2}}(2n_2-m)} \|0\rangle_{\rm ph}$	$\sqrt{\frac{\pi}{2}}$	11.1	6	EE	$\|{\rm H}\rangle_{\rm ph}^{\rm GKP}$
4	$\|0\rangle_{\rm ph}$	$\sum_{\alpha=0}^{2m} \sum_{\beta=0}^{2m} \sum_{\gamma=0}^{4m} \binom{2m}{\alpha}\binom{2m}{\beta}\binom{4m}{\gamma} (-1)^{\beta}$ $D_{\frac{1}{2}\sqrt{\frac{\pi}{2}}(\alpha+\beta-2m)} D_{\frac{i}{2}\sqrt{\frac{\pi}{2}}(\gamma-2m)} \|0\rangle_{\rm ph}$	$\frac{1}{4}\sqrt{\frac{\pi}{2}}$	0.4	96	EOE	$\|-\rangle_{\rm ph}^{\rm GKP}$
5	$S(\xi)\|0\rangle_{\rm ph}$	$\sum_{n_1=0}^{m} \binom{m}{n_1} D_{\sqrt{\frac{\pi}{2}}(2n_1-m)} S(r=1.1513, \theta=0)\|0\rangle_{\rm ph}$	$\sqrt{\frac{\pi}{2}}$	31.3	3	E	$\|0/1\rangle_{\rm ph}^{\rm GKP}$
6	$\|0\rangle_{\rm ph}$	$\sum_{n_1=0}^{2m} \sum_{n_2=0}^{2m} \binom{2m}{n_1}\binom{2m}{n_2} D_{e^{2i\pi/3}\sqrt{\frac{\pi}{\sqrt{3}}}(n_1-m)} D_{\sqrt{\frac{\pi}{\sqrt{3}}}(n_2-m)} \|0\rangle_{\rm ph}$	$\frac{1}{2}\sqrt{\frac{\pi}{\sqrt{3}}}$	2.6	44	EE	$\|0\rangle_{\rm ph}^{\rm GKP}$
7	$\|0\rangle_{\rm ph}$	$\sum_{n_1=0}^{m} \sum_{n_2=0}^{m} \sum_{n_3=0}^{m} \binom{m}{n_1}\binom{m}{n_2}\binom{m}{n_3}$ $D_{\sqrt{\frac{\pi}{\sqrt{3}}}(2n_1-m)} D_{e^{2i\pi/3}\sqrt{\frac{\pi}{\sqrt{3}}}(2n_2-m)} D_{e^{4i\pi/3}\sqrt{\frac{\pi}{\sqrt{3}}}(2n_3-m)} \|0\rangle_{\rm ph}$	$\sqrt{\frac{\pi}{\sqrt{3}}}$	9.5	6	EEE	$\|{\rm T}\rangle_{\rm ph}^{\rm GKP}$
8	$S(\xi)\|0\rangle_{\rm ph}$	$\sum_{n_1=0}^{m} \binom{m}{n_1} D_{\sqrt{\frac{\pi}{\sqrt{3}}}(2n_1-m)} S\left(r=1.64, \theta=\frac{\pi}{6}\right)\|0\rangle_{\rm ph}$	$\sqrt{\frac{\pi}{\sqrt{3}}}$	27.3	4	E	$\|0/1\rangle_{\rm ph}^{\rm GKP}$
9	$\|0\rangle_{\rm ph}$	$\sum_{\alpha=0}^{m} \sum_{\beta=0}^{\alpha} \sum_{\gamma=0}^{m-\alpha} \binom{m}{\alpha}\binom{\alpha}{\beta}\binom{m-\alpha}{\gamma} e^{-\frac{i\pi}{2}(2\beta-\alpha)(2\gamma+\alpha-m)}$ $D_{\sqrt{\frac{\pi}{2}}((2\beta-\alpha)+i(2\gamma+\alpha-m))} \|0\rangle_{\rm ph}$, $\sum_{\alpha=0}^{m} \sum_{\beta=0}^{\alpha} \sum_{\gamma=0}^{m-\alpha} \binom{m}{\alpha}\binom{\alpha}{\beta}\binom{m-\alpha}{\gamma} (-1)^{m-\alpha} e^{-\frac{i\pi}{2}(2\beta-\alpha)(2\gamma+\alpha-m)}$ $D_{\sqrt{\frac{\pi}{2}}((2\beta-\alpha)+i(2\gamma+\alpha-m))} \|0\rangle_{\rm ph}$	$\sqrt{\frac{\pi}{2}}$	11.5	6	$\|{\rm comb}_4^0\rangle$ or $\|{\rm comb}_4^2\rangle$	$\|H\rangle_{\rm ph}^{\rm GKP}$

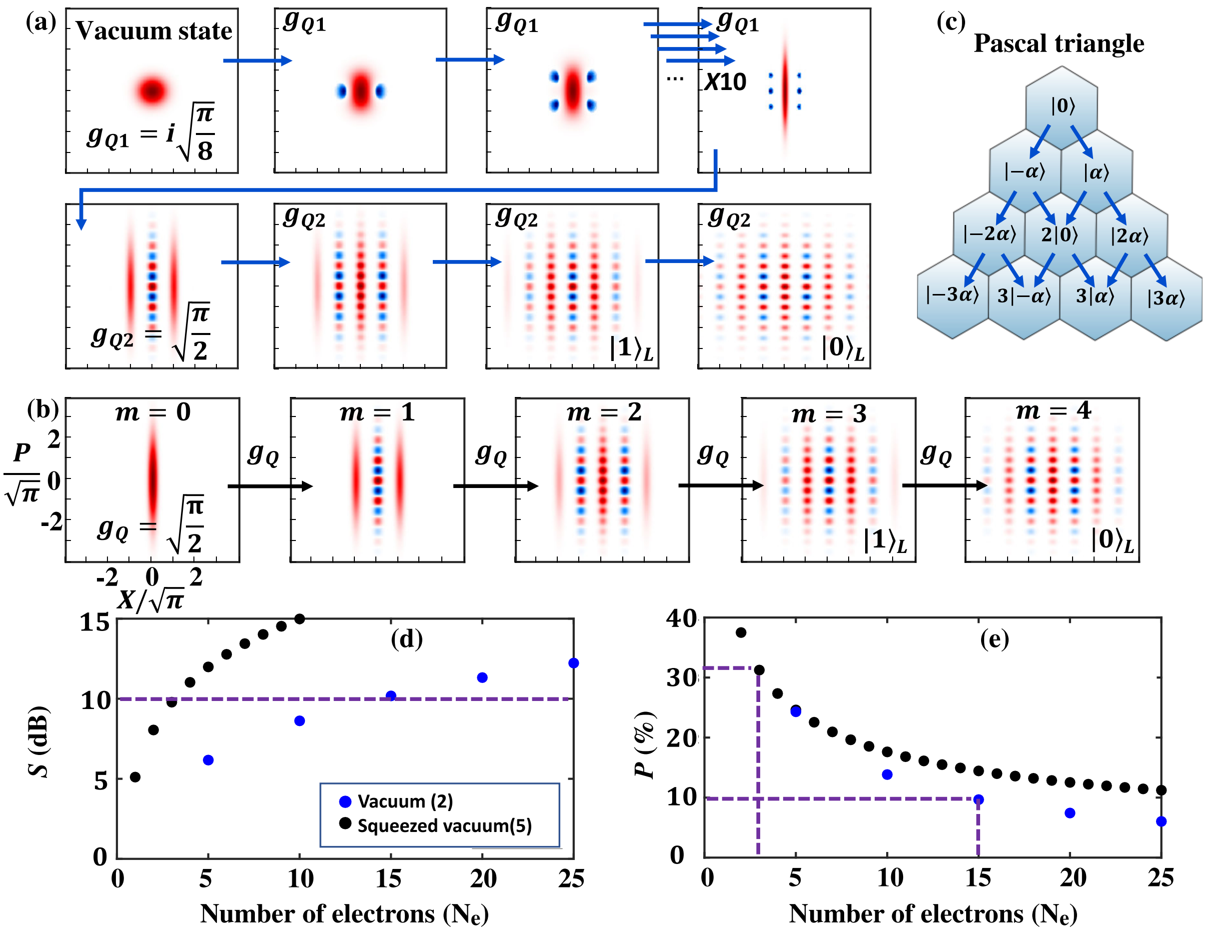

FIG. 3. A scheme for creation of the GKP state: squeezing and postselection probability. (a) The evolution of the Wigner function of the photonic state after each electron interaction and postselection. The first interactions all have the same coupling constant $g_{Q1} = i\sqrt{\pi/8}$, together squeezing the vacuum state. We then shift the phase of the interaction by $\pi/2$, so the later interactions all have a coupling constant $g_{Q2} = \sqrt{\pi/2}$ transforming the squeezed-vacuum state into a GKP state. (b) Creation of GKP state directly from an initial squeezed-vacuum excitation, i.e., seeding the electron-photon interaction with a squeezed vacuum in the optical mode. The GKP state is alternating between the approximated $|0\rangle_{\text{ph}}^{\text{GKP}}$ and $|1\rangle_{\text{ph}}^{\text{GKP}}$, showing that each interaction resembles the X gate for the GKP states. (c) The coefficients of the photonic state at every step of the process are described analytically using a Pascal triangle. This description simplifies the calculation of the postselection probabilities in Eq. (6) (Supplemental Material [85] Sec. IV). (d),(e) The squeezing parameter and postselection probability of the final GKP state as a function of the number of electron interactions: comparing photonic initial conditions of vacuum (a) and squeezed vacuum (b).

which the electron interacts. For electrons with the same coupling-constant phase, the order of interaction and order of postselection do not matter because displacement with similar directions are commutative. This fact greatly simplifies the current scheme and the ones below.

The resulting approximated GKP state is (Supplemental Material [85] Sec. III. 3)

$$|\text{GKP}'\rangle_{\text{ph}}^{m} \propto \sum_{n_1=0}^{m} \sum_{n_2=-0}^{4m} \binom{m}{n_1} \binom{4m}{n_2} \times D_{\sqrt{\frac{\pi}{2}}(2n_1-m)} D_{i\sqrt{\frac{\pi}{2}}(n_2-2m)} |0\rangle_{\text{ph}}. \tag{5}$$

For an even or odd m, this state approximates the ideal GKP of a logical zero or one state $|0\rangle_{\text{ph}}^{\text{GKP}}/|1\rangle_{\text{ph}}^{\text{GKP}}$. We recall that the ideal GKP states can be written as [86,87]

$$|\mu\rangle_{\text{ph}}^{\text{GKP}} \propto \sum_{\vec{n}\in\mathbb{Z}} D_{\sqrt{\frac{\pi}{2}}(2n_1+\mu)} D_{i\sqrt{\frac{\pi}{2}}n_2} |0\rangle_{\text{ph}}, \tag{6}$$

where $\mu = 0/1$ defines the logical GKP qubits $|0\rangle_{\text{ph}}^{\text{GKP}}/|1\rangle_{\text{ph}}^{\text{GKP}}$, respectively. When the number of electrons m approaches infinity, the approximated state [Eq. (5)] approaches the ideal GKP [Eq. (6)]. To calculate the squeezing of the approximated state, we rewrite Eq. (5)

in the x-quadrature representation (more details including the p-quadrature are found in Supplemental Material [85] Sec. III. 3):

$$\mathrm{GKP}'(x) \propto \sum_{n_1=0}^{m} \binom{m}{n_1} \cos^{4m}[\sqrt{\pi}(x+m\sqrt{\pi})/2] \times e^{-\frac{1}{2}[x-\sqrt{\pi}(2n_1-m)]^2}. \quad (7)$$

Equation (7) describes a series of peaks with a distance of $2\sqrt{\pi}$ shifted by $0\backslash\sqrt{\pi}$ for even or odd m. We note that the $\cos^{4m}$ term closely approximates a comb of Gaussian peaks (instead of delta functions). The squeezing parameter is given by the variance of the peaks (of the corresponding probability distribution), which scales like $\Delta_x^2 \cong 1/(1+\pi m)$. The corresponding squeezing parameter is defined as $S_{\mathrm{dB}} = 10\log_{10}(1/\Delta_x^2) = 10\log_{10}(1+\pi m)$, which thus grows logarithmically in the number of electrons. We choose m interactions for g_{Q2} and $4m$ for g_{Q1} such that the squeezing is similar in the x and p representations. This way, Figs. 3(d) and 3(e) can present a single squeezing parameter by showing a data point every five electron interactions. The ideal GKP $|\mu\rangle_{\mathrm{ph}}^{\mathrm{GKP}}$ is obtained at the limit of $m \to \infty$. Substituting $m = 3$ shows that $N_e = 15$ electrons are required to achieve approximately 10 dB squeezing [Fig. 3(d)], which is the estimated squeezing level for fault-tolerant quantum computing (reaching the quantum error-correction threshold) using CVs [88,89].

The postselection probability to obtain the state $|\mathrm{GKP}'\rangle_{\mathrm{ph}}^{m}$ is (illustrated in Fig. 3(e) and detailed in Supplemental Material [85] Sec. IV. 3)

$$P_{|\mathrm{GKP}'\rangle_{\mathrm{ph}}^{m}} = \frac{\|(D_{\sqrt{\pi/2}} + D_{-\sqrt{\pi/2}})^m (D_{i\sqrt{\pi/8}} + D_{-i\sqrt{\pi/8}})^{4m} |0\rangle_{\mathrm{ph}}\|^2}{4^{5m}}. \quad (8)$$

The postselection probability to produce the GKP of 10 dB squeezing ($m = 3$) according to Eq. (8) is approximately 10% [Fig. 3(e)]. As expected, the probability in Eq. (8) decreases for larger m, i.e., for a larger number of electrons N_e. However, the probabilities decay rather slowly with N_e, like approximately $5/(N_e\pi)$ (Supplemental Material [85] Sec. IV. 3), which leaves us with relatively high success rates. This fact may seem somewhat surprising when recalling that the success probability of postselecting the first electron is close to 50%, and that multiple postselections often scale exponentially in this probability. An exponential scaling would have caused the entire scheme to be impractical, and thus it is highly encouraging to instead find a power-law scaling in the number of electrons.

To increase the success probability of creating a GKP state further, one can stimulate the interaction with a squeezed-vacuum state [Fig. 3(b)]. We consider a squeezed-vacuum state in the initial photonic mode before the interaction $|\psi_i\rangle_{\mathrm{ph}} = S(\xi)|0\rangle_{\mathrm{ph}}$, with $S(\xi)$ being the squeezing operator $\exp(\frac{1}{2}\xi^* a^2 - \frac{1}{2}\xi a^{\dagger 2})$, and $\xi = re^{i\theta}$ being the squeezing parameter [8]. For seeding a squeezed vacuum into the optical mode, one can use mature techniques like spontaneous parametric down-conversion or spontaneous four-wave mixing. After the interaction of N_e electrons with the squeezed-vacuum state (where $g_{\mathrm{Q}} = \sqrt{\pi/2}$, $\theta = 0$), the resulting photonic state becomes (Supplemental Material [85] Sec. III. 4)

$$|\mathrm{GKP}''\rangle_{\mathrm{ph}}^{N_e} \propto \sum_{n=0}^{N_e} \binom{N_{\mathrm{e}}}{n} D_{\sqrt{\frac{\pi}{2}}(2n-N_e)} S(\xi)|0\rangle_{\mathrm{ph}}, \quad (9)$$

which is an approximation of GKP states [22]. Writing Eq. (9) in the p representation:

$$\mathrm{GKP}''(p) \propto \exp\left(-\frac{p^2}{2}e^{-2r}\right)(1+e^{-2i\sqrt{\pi}p})^{N_e}. \quad (10)$$

A comparison with the x representation is discussed in Supplemental Material [85] Sec. III. 4. The probability of postselecting all electrons with even energies is (Supplemental Material [85] Sec. IV. 4)

$$P_{|\mathrm{GKP}''\rangle_{\mathrm{ph}}^{N_e}} = \frac{1}{4^{N_e}} \sum_{n=0}^{2N_e} \binom{2N_e}{n} e^{-\pi(N_e-n)^2|\cosh r + \sinh r|^2}. \quad (11)$$

The probability here decays more slowly, like $1/\sqrt{N_{\mathrm{e}}\pi}$, because there is one axis rather than two for the displacement interactions.

We calculate the squeezing parameter of the optical GKP state as a function of the number of electrons N_e and find $S_{\mathrm{dB}} = 10\log_{10}(e^{-2r} + N_e\pi)$ (Supplemental Material [85] Sec. III. 4). To achieve 9.8-dB squeezing for the GKP state [Fig. 3(d)], we need just three electrons. The postselection probability to produce this state according to Eq. (11) is 31.25% [Fig. 3(e)].

The reason for the relatively high success probabilities is that the electron-photon scattering matrix S of Eq. (1) causes the quantum state to gradually converge into the ideal GKP states. The closer the photonic state reaches, the better the success probability becomes. Destructive interference in the electron wave function reduces the

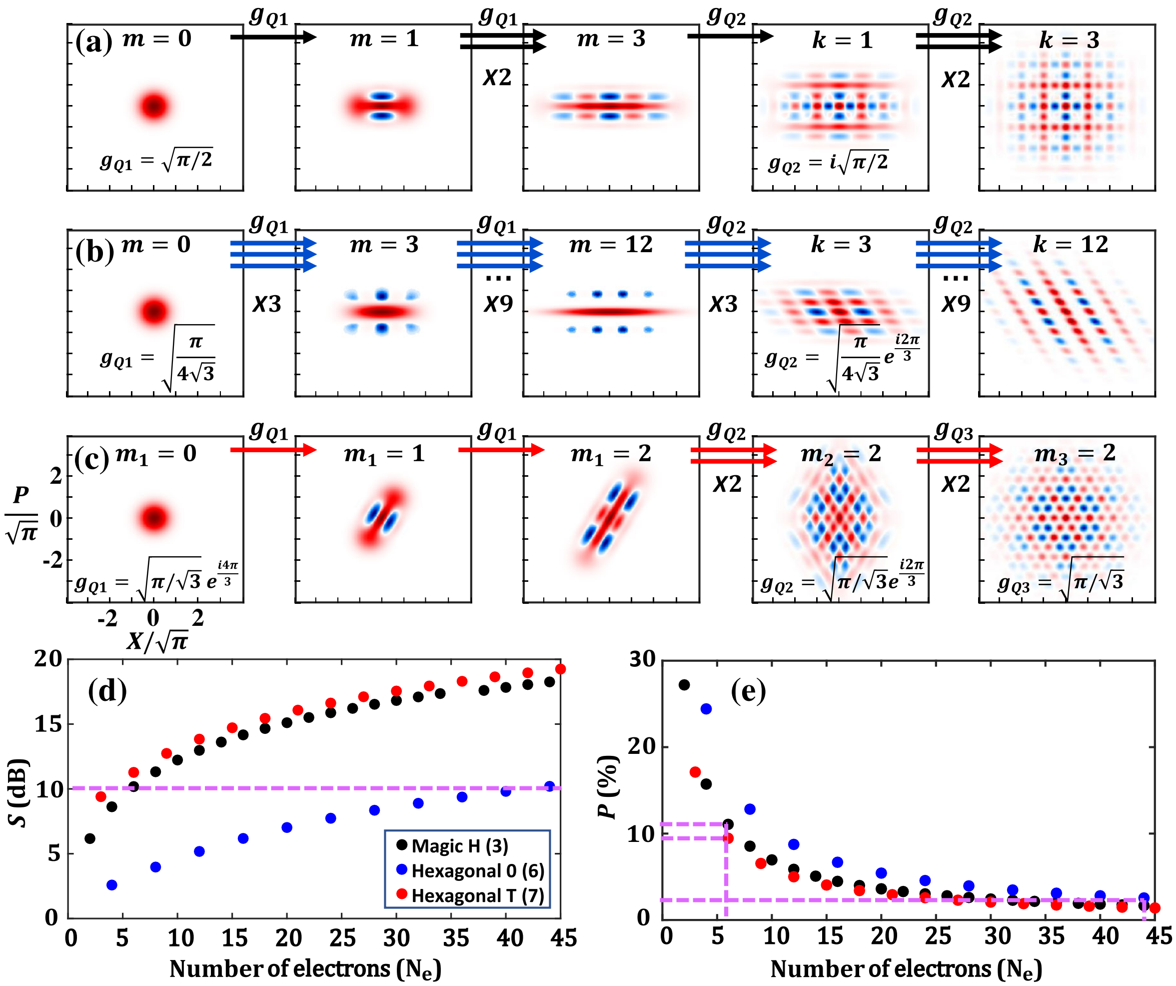

FIG. 4. Schemes for the creation of different GKP states and their characterization. (a) Creation of the magic GKP state $|\mathrm{H}\rangle_{\mathrm{ph}}^{\mathrm{GKP}}$ (third row in Table I). (b) Creation of the hexagonal-GKP state $|0\rangle_{\mathrm{L}}$ (sixth row in Table I). (c) Creation of the hexagonal magic state $|\mathrm{T}\rangle_{\mathrm{ph}}^{\mathrm{GKP}}$ (seventh row in Table I). (d),(e) The squeezing parameter and postselection probability of the GKP states in (a)–(c) as a function of the number of electrons.

probability of the electron acquiring odd energies after the interaction, and thus increases the postselection probability. The sequential application of the electron interaction and postselection (with the coupling constant $g_{Q2} = \sqrt{\pi/2}$) causes a convergence into the GKP states, shifting between the $|0\rangle_{\mathrm{ph}}^{\mathrm{GKP}}$ and the $|1\rangle_{\mathrm{ph}}^{\mathrm{GKP}}$ GKP states for an even and odd number of interactions, respectively. Using the terminology of quantum-error correction, two consequent interactions are a stabilizer for the GKP state [11] (Supplemental Material [85] Sec. VII). We find a similar convergence for the other GKP states for different interaction parameters as listed in Table I. In all these cases, the interactions with comb electrons define stabilizers for the corresponding GKP states, making such fundamental interactions precisely suited for the creation of GKP states.

D. Creation of hexagonal-GKP and magic states

Our approach enables the creation of additional types of GKP states such as the hexagonal GKP [Fig. 4(b)]. Examples are summarized in Table I, each requiring different coupling constants with different relative phases between the sets of interactions. The magic GKP states [Figs. 4(a) and 4(c)], first proposed by Ref. [90], enable universal quantum computation without requiring additional non-Gaussian elements [91]. We show how magic states can be created by using comb electrons. For example, for the square-GKP magic state $|\mathrm{H}\rangle_{\mathrm{ph}}^{\mathrm{GKP}}$ shown in Fig. 4(a), we propose a scheme involving $N_e = 2m$ electrons (presented in the third row of Table I): having m interactions with coupling $g_{Q1} = i\sqrt{\pi/2}$ postselected for even energies, followed by additional m interactions with coupling $g_{Q2} = \sqrt{\pi/2}$ postselected for even energies. Similarly, the hexagonal-GKP magic state $|\mathrm{T}\rangle_{\mathrm{ph}}^{\mathrm{GKP}}$ shown in Fig. 4(c) can be created as shown in the seventh row of Table I.

In all these schemes, the electron state could be thought of as the analog of an ancilla qubit performing a conditional displacement, which was shown to create GKP states in different physical systems [17,18]. However, the electron interaction can also go beyond the existing proposals for GKP generation by creating states that have no analog with an ancilla qubit.

Indeed, the ninth row of Table I describes the creation of GKP magic states using $|\mathrm{comb}_4^0\rangle_\mathrm{e}$, i.e., electron comb separated by $4\hbar\omega$, reaching 10 dB squeezing with six electrons of this type. This electron state can simplify the creation of magic states and certain operations on GKP states such as entangling gates between two GKP qubits. Interestingly, such an electron comb with higher-energy spacing is no longer analogous to an ancilla qubit but is instead analogous to an ancilla qudit (e.g., $|\mathrm{comb}_4^0\rangle_\mathrm{e}$ is the analog of a four-level system). Such electron combs provide additional degrees of freedom, such as conditional displacements with qudit states, opening new possibilities for generation of CV states, various gate operations, and error-correction protocols with fewer electrons or a simpler preparation. It could be intriguing to translate these concepts to other areas of quantum information and propose analog qudit implementations in trapped ions and circuit QED.

E. Creation of entangled GKP states: Toward cluster states

It is insightful to recast the electron-photon interaction to the language of quantum gates. Specifically, the same comb electrons used above to create the GKP state enable implementing quantum gates such as the Pauli X, Y, and Z for the GKP states (Supplemental Material [85] Sec. VII). We now combine this approach with the ideas developed in Ref. [92] to induce entanglement between two photonic modes. A free-electron interaction with two photonic modes can entangle them by performing two-qubit gates (e.g., controlled NOT), creating a GKP Bell state. To see that, we consider an electron that interacts with two photonic modes, e.g., by placing two cavities along the electron trajectory. The combined interaction is then described by two scattering matrices S_1,S_2, each related to the interaction with a different photonic mode. The free electron acts as a flying qubit, allowing the entanglement of multiple GKP states along its trajectory. This is a desired property for quantum hardware with high connectivity for creating shallow quantum circuits [93,94].

As an example, consider the following initial state:

$$|\psi_{\mathrm{initial}}\rangle = |\mathrm{comb}_4^0\rangle_\mathrm{e}|0\rangle_{\mathrm{ph1}}^{\mathrm{GKP}}|0\rangle_{\mathrm{ph2}}^{\mathrm{GKP}}, \tag{12}$$

which corresponds to an (qudit) electron comb with a spacing of $4\hbar\omega$ and two photonic modes ($|0\rangle_{\mathrm{ph1}}^{\mathrm{GKP}}$, $|0\rangle_{\mathrm{ph2}}^{\mathrm{GKP}}$) in a GKP state. Following the interaction of this electron comb with both modes, we postselect the electron energy. The result is (see Supplemental Material [85] Sec. VI)

$$\begin{cases} |+\rangle_{\mathrm{ph1}}^{\mathrm{GKP}}|+\rangle_{\mathrm{ph2}}^{\mathrm{GKP}} + |-\rangle_{\mathrm{ph1}}^{\mathrm{GKP}}|-\rangle_{\mathrm{ph2}}^{\mathrm{GKP}}, & \text{for postselecting } |\mathrm{comb}_4^0\rangle_e, \\ |+\rangle_{\mathrm{ph1}}^{\mathrm{GKP}}|-\rangle_{\mathrm{ph2}}^{\mathrm{GKP}} - |-\rangle_{\mathrm{ph1}}^{\mathrm{GKP}}|+\rangle_{\mathrm{ph2}}^{\mathrm{GKP}}, & \text{for postselecting } |\mathrm{comb}_4^2\rangle_e. \end{cases} \tag{13}$$

Both options are GKP Bell states. Postselecting the electron will generate one of these Bell states according to the measured electron energy. The electron state $|\mathrm{comb}_4^0\rangle_\mathrm{e}$ acts like a conditional rotation gate for the GKP square state (similarly, for the hexagonal-GKP state, a $|\mathrm{comb}_6^0\rangle_\mathrm{e}$ can be used).

Looking forward, it is important to consider prospects of scaling up our scheme, aiming toward the generation of multimode entangled GKP states. Increasing the rate of GKP generation can be done through temporal or spatial multiplexing. Above-GHz electron-pulse rates can be achieved using GHz streaking cavities or using photoemission with high-repetition-rate fs lasers. Alternatively, a cathode array can be used to generate parallel electron beams that interact with parallel waveguides.

Both temporal and spatial multiplexing [95–98] can facilitate the creation of entanglement between GKP states, toward the vision of a GKP cluster state. Specifically, multiplexing in time can be used to create cluster states [99]. Multiplexing in space of neighboring modes can be done using configurable electron-beam splitters. Lastly, electrons can also interact with multiple modes in parallel or sequentially, allowing yet unexplored ways for entangling different optical modes.

F. Fidelity estimation

We now turn to estimate the fidelity of the cat and GKP states. Different considerations can lower the fidelity in practical settings, including detector efficiencies, deviation from the ideal comb, variance in the constant coupling g_Q, the bandwidth of the optical mode (or multimode), dispersion of either the electron or the photonic modes, aberrations for the temporal and transversal electron-beam focusing, and electron-electron repulsion. That said, we can give a strong indication of the robustness of the proposed approach. Consider a standard deviation Δg_Q in the value of g_Q (the variation is taken to be in the amplitude for this example). Such deviations in PINEM experiments result, for example, in transverse nonuniformities in the field

$E_z(r_\perp, z)$. We find that the fidelity for the case of a two-component cat state goes like $\propto 1 - \Delta g_Q^2$, with $\Delta g_Q < 0.25$ [Sec. V. 5 and Fig. 1(b) in the Supplemental Material [85]].

We consider whether our approach is limited by decoherence times (i.e., T_1, T_2). The free electron is a fundamental particle, and thus in freespace it does not experience decay by spontaneous emission like atoms, ions, and superconducting qubits. For example, T_1-like effects could result from interactions of electrons with their environment inside the electron microscope. These interactions involve excitations of current loops in the tubes and thermal-magnetic field noise [100], which are at frequencies much lower than the optical range that we analyze here, and are thus negligible. In contrast, the interaction of electrons with unwanted modes and excitations [101] (e.g., surface plasmons, phonons, other waveguide modes) in the structure may seriously affect the coherence of the electrons. According to a recent work [102], these multimode effects could be optimized to be as small as possible by designing the geometry and refractive indices of the waveguide appropriately.

T_2 effects are partially analogous to electron dispersion because dispersion changes the phases of the electron energy components. Such phase changes deform the electron comb, reducing the fidelity of the generated photonic state. Our calculations consider the effect of electron dispersion, which, for example, imposes an upper limit on the interaction length. T_2 effects may also arise from spontaneous emission in the shaping process by randomly broadening the energy peaks of the comb, creating uncertainties in its phase after propagation. Another potential source of T_2-type decoherence is the distortion of the comb's phases by electron optics [103] smearing the comb due to different path lengths in the electron beam (the electron path on the perimeter of the beam traveling a longer path relative to the center of the beam). This effect may limit consequent interactions of the same electron with multiple cavities, depending on the quality of the comb at the Talbot distance and depending on the optimization of the electron optics to minimize temporal aberrations.

We note that there is a difference between dispersion and T_2 since the dispersion of the electron is not a random process and does not involve coupling to external degrees of freedom (like a bath). The dispersion can be utilized to shape the electron wave function and is in fact essential to the generation of electron combs. Moreover, due to the quantum Talbot effect, the deformation of the electron comb is reversed at certain distances, leading to multiple revivals of the comb (eventually limited by the ratio $\hbar\omega/\sigma_e$). These quantum revivals are somewhat analogous to the spin-echo effect yet arising through propagation and without requiring coherent-control pulses.

The fidelity is also limited by the quality of the comb electron. Any Gaussian comb has two characterizing features: its envelope width and the energy width of the individual peaks (coherent and incoherent broadening). The width of each energy peak can create an error in the detection due to some overlap between adjacent peaks. For high fidelity, the ratio between the energy of the photon and the standard deviation of each peak should be above 3 standard deviations for error rates below 1%. For the telecom range, the photon energy is 0.8 eV; this means that the standard deviation of the electron energy width of each peak should be approximately 0.13 eV (approximately 0.3 eV FWHM), which is achievable in TEM and even UTEM [104]).

Another consideration is the finite-energy width of realistic electron combs that approximate the infinite width of the ideal comb. A wider electron comb increases the fidelity [Sec. V. 3 and Fig. 2(h) in the Supplemental Material [85]], but only up to a certain propagation distance, because a wider comb experiences stronger dispersion that distorts the phases of the comb peaks, limiting the fidelity. Strong coupling ($g_Q > 0.5$), as necessary for GKP generation, requires long phase-matched interactions [64–66,105] on the order of 100 μm (for 200 keV electron combs and photons of 1550 nm). Since the phase distortion by dispersion grows linearly with the distance (Supplemental Material [85] Sec. V. 6), there exists a different optimal electron energy width for each interaction distance and each required fidelity; i.e., too wide a comb will in fact smear the phase due to electron dispersion, resulting in lower fidelities [Sec. V. 6 and Fig. 1(c) in Supplemental Material [85]]. These considerations create an inherent trade-off between the fidelity and coupling strength g_Q. Our results show that despite this trade-off, there is a wide range of parameters for which we can create the photonic states necessary for CV fault-tolerant quantum computing.

The fidelity of the generated GKP state depends on the electron detection efficiency and the electron number distribution. Assuming that the electron number distribution follows Poisson statistics with parameter λ (which can be controlled, for example, by the intensity of a laser triggering electron photoemission), the optimal λ in terms of the probability of getting a GKP with squeezing above 10 dB is $\lambda = 5$. To estimate the fidelity for each postselected state, we further include the electron detection efficiency η in the calculation. Typical electron detection efficiencies in hybrid pixel direct electron detector cameras [41,106,107] are $\eta = 0.95$ and can be as high as $\eta = 0.99$, yielding a lower bound on the fidelity of 95% (Supplemental Material [85] Sec. V. 7).

To provide concrete fidelity estimates for GKP states created by approximated electron combs, we consider a Gaussian envelope for the electron energy spectrum as in Ref. [76]. The Gaussian envelope is preferable since it maximizes the first moments while minimizing higher-order moments of the electron energy spectrum. We estimate that creating an approximate GKP state [Eq. (5)] with 98% fidelity requires a standard deviation of 30 peaks (Supplemental Material [85] Sec. V. 5). As an example, we consider such an electron with mean kinetic energy of

200 keV. We choose the distance between the electron energy peaks to match the energy of a photon at 775 nm, so the emission is into a GKP state at 1550 nm. The fidelity of the GKP state created by such a comb can remain above 97% for an interaction distance of up to 160 μm. Such a distance is sufficient to create the strong-coupling strength g_Q as was predicted in Ref. [78] and shown in Ref. [105]. These papers and the others discussed below show that each of the necessary components toward the realization of our proposal has been demonstrated in a separate experiment in recent years. Taken together, these advances help us envision a roadmap toward the full experimental demonstration of free-electron generation of optical GKP states.

III. DISCUSSION

A. Roadmap toward an experimental realization

The realization of free-electron-driven optical GKP states requires addressing important challenges in each of the three stages of the process [Figs. 1(a)–1(c)].

First, in the preparation stage [Fig. 1(a)], multiple harmonics [75] or multiple interactions [76] are necessary to shape the electrons into high-quality combs. Recently, strong electron shaping with a continuous-wave laser was demonstrated [70,71], instead of the short laser pulses used in previous experiments of this kind [47–52,61,63,65]. This mode of operation allows for coherent electron shaping (i.e., temporal modulation) with less complicated synchronization for the interactions between the electron and the shaping light. However, for the continuous-wave interaction to be efficient enough (the combs we consider in Fig. 1 of Sec. V. 6 in the Supplemental Material [85] have coupling $g = \sqrt{N} g_{\mathrm{Q}} \sim 50$, with N being the mean number of photons), Refs. [70,71] utilized grazing angle conditions for phase-matched or quasi-phase-matched interactions. Such grazing angle conditions require strong electron lenses to create a small electron-beam diameter together with small convergence angles. These conditions can be met in TEMs, which provide such lenses, in addition to the required deflectors, electron spectrometer, and a fast camera.

Another important consideration that may limit experimental realizations is that the shaping method itself can reduce the electron-beam quality by introducing transverse-momentum components. For example, if the shaping is performed using a PINEM interaction with a mirror [61], each photon emitted or absorbed will give the electron a transverse kick on the order of 10 μrad. In our case, we talk about a few dozen photons absorbed or emitted during the interaction, which will result in a few-hundred-μrad deflection. To reduce this effect, the comb preshaping could be done with light that has momenta primarily along the electron propagation direction, such as in certain optical waveguides.

Second, the light-emission stage [Fig. 1(b)] requires strong coupling ($g_{\mathrm{Q}} > 0.5$) between the electrons and the optical mode, together with suppression of interaction with the nondesired modes (close to unity ideality, as analyzed in Ref. [102]). The highest g_{Q} reported so far was close to unity [105], which is at the scale of the values needed for GKP generation. Such a g_{Q} value was demonstrated using a structure supporting hybrid modes of surface-plasmon polaritons and photons in a waveguide [105]. The disadvantage of this scheme is the lossy nature of such polaritons. Theoretical proposals for similar coupling efficiencies with smaller losses are based on electron interaction with microcavities [78], or with photonic crystal flat bands [108]. The value of g_{Q} can be further increased, even much above unity, using a longer phase-matched interaction and a highly confined optical mode [78]. Phase-matched electron interaction lengths of up to 500 μm have been demonstrated [65], while maintaining its coherence [66]. We estimate that an interaction of about 150 μm is required for a large enough g_{Q}, while still maintaining low enough distortions of the comb phase due to dispersion accumulated during the propagation. Moreover, the optical mode must have a substantial part of its energy in vacuum and have a longitudinal polarization to ensure efficient evanescent coupling to the electron (as shown in Ref. [105]).

These interaction conditions also depict the timescale over which the emission occurs, which in the case of a 60 μm structure and 200 keV electrons is approximately 800 fs. This timescale also corresponds to the bandwidth of the emitted radiation, which is then about 10 nm for emission at 1550 nm. The photonic losses should be negligible over the interaction length and timescale, as is indeed the case in state-of-the-art dielectric waveguides and microcavities. Typical losses in the range of 0.1–1 dB/cm are negligible for an interaction extending over less than a millimeter. Other losses that arise from out-coupling could be mitigated as in other photonic technologies (quantum and classical).

An important consideration for the light emission stage is the requirement that the electron interacts predominantly with one optical mode; i.e., the electron coupling strength (g_{Q}) with a specific mode is much larger than with other modes. To satisfy this condition, we can rely on established electromagnetic simulations, like the ones used in electron energy-loss spectroscopy (EELS) [81], which are known to show good agreement with experiments [41,50,70,71]. Finding a satisfactory structure design can be achieved by exploiting optimization methods from nanophotonics such as dispersion engineering and photonic inverse design [109]. Interestingly, a recent paper [105] showed a hybrid photonic-plasmonic structure with coupling of order unity into a single mode (so far, relatively broadband and lossy). Another recent paper [102] optimized over designs of silicon-nitride-on-silica waveguides, finding a concrete low-loss design with coupling of order unity. This Ref. [102] also shows that coupling ideality to a single mode can be above 0.9 (so far, at the expense of weaker coupling). It is still an open question to find the fundamental laws that govern the designs of such structures and their limits in the most general case.

Even for multimode structures that are far from having ideal coupling to a single mode, we can enhance the interaction with a single desired mode by pumping it with a weak coherent state, or a weakly displaced squeezed vacuum. An alternative solution is creating the GKP states such that each photon is a superposition of multiple spectral modes. In such a scenario, the coherent width of each electron energy peak needs to be wider than the spectral width of the photoemission. The coherent energy width of electrons emitted from typical cathodes is on the order of 0.3 eV [110,111]. To keep this value wider than the spectral width of the photon emission, a minimal phase-matched interaction length of approximately 30 μm is required, which fits well with the other constraints of typical experiments in this field.

We propose two platforms for experimental realizations, depending on the desired technique in quantum-information processing. For measurement-based computation schemes, the electron can radiate the light directly into an integrated open waveguide. This waveguide can later be brought to interact with other waveguides, to create entanglement between multiple GKP states, form a cluster, and eventually perform quantum computation or communication. These kinds of platforms are the ones sought after, for example, by Ref. [112]. This approach necessitates multiple electrons per pulse for GKP generation or single-electron pulses for multicomponent cat-state generation. Open photonic waveguides support a relatively wide emission bandwidth. This allows, in principle, for production of GKP states with high repetition rates (limited by the electron emission rates). However, the high rate comes at the price of a more complicated dispersion engineering throughout the photonic chip.

In contrast, for gate-based quantum computation, the electron can radiate into a waveguide that is part of a microcavity. In this case, we envision multiple electrons brought on demand to interact with the same photonic mode, performing multiple operations on it, without affecting the coherence time of the cavity (thus avoiding the reduction of coherence when coupling ancilla qubits to cavities in other platforms such as circuit QED). As we will discuss in a future work, such systems can use electrons to implement nonlinear operations that control and entangle the cavity modes, even in spatially separated cavities [92]. The quality factor of the microcavity will be decided by the need to satisfy the phase-matching condition and the need to maximize the coupling strength g_Q, limiting the lifetime of the encoded GKP state.

Third, the electron postselection stage [Fig. 1(c)] necessitates coincidence measurements and direct detection of individual electrons. Such measurements are already possible due to advances in electron-counting direct detectors. Recent experiments reported coincidence of electron energy loss with x-ray emission [113] and with optical photon emission [41,77] using single-photon detectors. One advantage of free-electron generation of GKP states arises from the developments in fast electron-counting detectors (direct-detection schemes). Since free electrons are energetic particles, the bounds on their detection efficiency are completely different from those for photons. Because of this fundamental difference, it should ultimately be easier to achieve a simultaneous detection of multiple electrons than to achieve a similar photon-counting detection with photons.

B. Analogies between electron-photon and photon-photon interactions

Let us follow the approximate analogy between Eq. (1) and a beam splitter. We can "translate" the electron to an approximate harmonic oscillator to compare our proposed protocols with the known approaches for creation of GKP using beam splitters and postselection [22,24–26,34]. This kind of translation helps in emphasizing the advantage of the free-electron platform: Experiments with electrons enable the creation of states that are extraordinarily hard to make with photons in the optical range.

The monoenergetic electron state $|n\rangle_{\mathrm{e}}$ is analogous to a Fock state of many photons (high enough in the harmonic-oscillator ladder so that $aa^\dagger|n\rangle_{\mathrm{ph}}^{\mathrm{Fock}} \approx a^\dagger a|n\rangle_{\mathrm{ph}}^{\mathrm{Fock}}$). The states we define as $|\mathrm{comb}_2^i\rangle_{\mathrm{e}}$, $i = 0, 1$ are the electron analogs of intense Schrödinger cat states (with large amplitudes). We can see this analogy by noting that $b|\mathrm{comb}_2^{1,0}\rangle_{\mathrm{e}} = |\mathrm{comb}_2^{0,1}\rangle_{\mathrm{e}}$ as expected from even and odd cat states. This connection arises because the b and $b^\dagger$ electron operators are displacement operators on the electron wave function. Nevertheless, note that this analogy is not perfect and using a different perspective—looking at the Wigner functions—shows that the electron comb state is equivalent to the GKP state rather than the cat state.

Previous works in quantum optics found how to create optical GKP states using beam splitters and optical cat states [22]. However, these schemes rely on *a priori* generation of the cat states, which are difficult to generate reliably (especially with substantial photon numbers). Currently, to the best of our knowledge, there is no practical way to create such states with sufficient photon numbers for the GKP schemes. From this point of view, our free-electron scheme has certain advantages because the analog of the cat state is the comb electron, which several labs have already demonstrated experimentally [65,70,71]. The creation of a sufficient-quality comb electron is becoming a standard experiment, whereas the creation of an optical cat state of sufficient photon number is a formidable task.

Another important insight arising from this approximate analogy pertains to the postselection that is necessary in these schemes. Many schemes in the photonic case rely on the photon number resolving the detection. Such photonic measurements have a relatively low detection rate and suffer from high measurement errors, especially for large photon numbers. In contrast, the analogous measurement in the electron case is electron spectroscopy, which can measure the exact change in electron energy over a range of thousands of photons. This technology provides a substantial advantage over photonic detection, which, for example, enables high-repetition-rate generation of GKP states limited only by the electron emission rates. Additionally, since the electrons are very energetic particles (5 orders of magnitude above the optical photon energy), the quantum efficiency of their detection can be very close to unity.

C. Applications of the general concept in other physical systems

It is interesting to search for other opportunities to apply the schemes we develop here in places where a similar scattering matrix arises. Any physical mechanism that is described by such a scattering matrix may now be facilitated for the creation of quantum states of light. For example, a single-photon optical-frequency comb going through a $\chi^{(2)}$ medium can generate photonic-squeezed states at a frequency corresponding to half the difference between the spectral peaks of the comb (typically MHz to THz, depending on the frequency comb). The emitted photonic-squeezed state is then heralded by a spectrometry measurement of the frequency comb photon. If a large-enough $\chi^{(2)}$ could be achieved (corresponding to a large g_{Q}), our approach would enable us to directly create photonic GKP states using single-photon frequency combs.

Alternative routes of using the approach in this work are exploiting existing experiments that already create bunched electron pulses and beams. For example, above-threshold ionization and free-electron lasers create bunched-electrons beams that can often contain multiple electrons per bunch. We propose launching bunched electrons with temporal modulation of the $\pi/\hbar\omega$ state $|\mathrm{comb}_2^0\rangle_{\mathrm{e}}$ (i.e., energy spacing of $2\hbar\omega$) into an undulator with double the period ($2\pi/\hbar\omega$) to trigger electron radiation at frequency $\hbar\omega$. In such a scenario, our work predicts that the resulting undulator radiation will be squeezed and heralded by measuring the electrons' energy. This approach can create squeezed-x-ray states using highly relativistic electrons. Moreover, if a large effective g_{Q} can be achieved in undulators (e.g., using highly charged ions [114]), then such an undulator radiation would take the form of cat states and GKP states. This way, we envision future free-electron lasers that create cat states in spectral regions such as THz and x rays, where no other methods currently exist for the creation of such quantum states.

IV. SUMMARY AND OUTLOOK

In summary, this paper demonstrates how shaping and postselecting free electrons can generate N-component cat states and grid states that are desired for CV quantum-information processing. Furthermore, we show how multiple electrons can create GKP states in an approach that resembles breeding schemes [22,28,34]. Recent experimental achievements show the feasibility of our proposal, for example, the necessary preshaping of free electrons into wide coherent energy combs was demonstrated in several recent experiments [65,70,71]. Controlling the comb spacing can be achieved using a PINEM-type interaction driven by harmonics of the fundamental laser frequency [49,75] or by multiple points of interaction [76]. In future works, we envision combining transverse and longitudinal shaping to scale this scheme to large GKP cluster states.

Taking a wider perspective, the comb electrons can themselves encode quantum information, as shown by the recent proposal [115] and observation [69] of free-electron qubit schemes. We note that in terms of their Wigner functions, optical GKP states are equivalent to electron combs with a spacing of $2\hbar\omega$, where the logical $|0\rangle_{\mathrm{e}}$ ($|1\rangle_{\mathrm{e}}$) state is the even (odd) electron energy comb. This equivalence has certain similarities to the idea of encoding CV quantum information on a single-photon frequency comb [116]. Using this description, each comb electron can be thought of as an ancilla qubit, which through its interaction with the optical mode performs a conditional displacement on the photonic state.

Interestingly, the ability to perform a conditional displacement arises naturally from the fundamental interaction of free electrons, in contrast to other systems such as ion traps and circuit QED, where additional complexity is required to generate the needed effective interaction. For example, in trapped ions, such conditional displacement can be achieved using Mølmer-Sørensen gates [117,118], which requires arrangements of bichromatic fields and can induce significant phase instability. In circuit QED schemes, the conditional displacement arises from additional effective nonlinear terms in the dispersive regime [17], which can induce photon-dependent qubit dephasing, relaxation times, and other unwanted effects [119]. In the case of electrons, the nature of their interaction enables us to directly extend the concept of GKP creation and propose more advance schemes such as the creation of multicomponent cat states and GKP states [e.g., using $|\mathrm{comb}_4^0\rangle_{\mathrm{e}}$, as in Fig. 2(f) and Table I row 9]. The duration of free-electron interaction is relatively short, lasting only about a picosecond. This enables very swift gate operations that are limited only by electronics response times and laser repetition rates (subnanosecond scale in current technology). For comparison, consider the conditional displacement gate, which in circuit cavity QED typically takes approximately 1 μs [31], whereas in ion traps, it was so far shown to take hundreds of microseconds [18]. Nevertheless, such a comparison should also consider that lifetimes of optical modes (hundreds of nanoseconds) are significantly shorter than in circuit QED and in ion traps (hundreds of microseconds and milliseconds, respectively).

Therefore, for free electrons interacting with optical modes, the bottleneck for active error correction would probably lie in much faster electronics capable of decision-making with nanosecond timescale. The creation of conditional displacement, together with regular displacements, enable quantum-error correction of GKP qubits as in Ref. [17]. Single-qubit universal control of such electrons was shown in Ref. [115]. Combining such operations, our work provides a novel mechanism for quantum-error-correction schemes based on free-electron interactions. Such interactions provide the necessary components toward a vision of free-electron-assisted fault-tolerant photonic quantum computation in the optical region.

ACKNOWLEDGMENTS

We thank Asaf Diringer and Aviv Karnieli for the valuable conversations and insight. This research was funded in part by the Gordon and Betty Moore Foundation, through Grant GBMF11473. In addition, the research was supported by the European Research Council (ERC Starting Grant No. 851780-NanoEP), and the European Union Horizon 2020 Research and Innovation Program (under Grant Agreement No. 964591 SMART-electron). R. D. would like to acknowledge the support of the Council for Higher Education Support Program for Outstanding Ph.D. Candidates in Quantum Science and Technology in Research Universities. G. B. would like to acknowledge the support of the Technion Excellence Program for undergraduate students. I. K. and A. G. acknowledge the support of the Azrieli Fellowship. This research was supported by the Technion Helen Diller Quantum Center.

[1] L. Schächter, *Beam-Wave Interaction in Periodic and Quasi-Periodic Structures* (Springer, New York, 2013).
[2] G. R. Blumenthal and R. J. Gould, *Bremsstrahlung, Synchrotron Radiation, and Compton Scattering of High-Energy Electrons Traversing Dilute Gases*, Rev. Mod. Phys. **42**, 237 (1970).
[3] B. W. J. Mcneil and N. R. Thompson, *X-Ray Free-Electron Lasers*, Nat. Photonics **4**, 814 (2010).
[4] C. Pellegrini, A. Marinelli, and S. Reiche, *The Physics of X-Ray Free-Electron Lasers*, Rev. Mod. Phys. **88**, 015006 (2016).
[5] F. V. Hartemann, W. J. Brown, D. J. Gibson, S. G. Anderson, A. M. Tremaine, P. T. Springer, A. J. Wootton, E. P. Hartouni, and C. P. J. Barty, *High-Energy Scaling of Compton Scattering Light Sources*, Phys. Rev. ST Accel. Beams **8**, 100702 (2005).
[6] N. D. Powers, I. Ghebregziabher, G. Golovin, C. Liu, S. Chen, S. Banerjee, J. Zhang, and D. P. Umstadter, *Quasi-Monoenergetic and Tunable X-Rays from a Laser-Driven Compton Light Source*, Nat. Photonics **8**, 28 (2014).
[7] R. J. Glauber, *The Quantum Theory of Optical Coherence*, Phys. Rev. **130**, 2529 (1963).
[8] M. O. Scully and M. S. Zubairy, *Quantum Optics* (Cambridge University Press, Cambridge, England, 1999).
[9] S. Haroche and J. Raimond, *Exploring the Quantum: Atoms*, *Cavities and Photons* (Oxford University Press, New York, 2006).
[10] S. L. Braunstein and P. van Loock, *Quantum Information with Continuous Variables*, Rev. Mod. Phys. **77**, 513 (2005).
[11] D. Gottesman, A. Kitaev, and J. Preskill, *Encoding a Qubit in an Oscillator*, Phys. Rev. A **64**, 012310 (2001).
[12] Z. Leghtas, G. Kirchmair, B. Vlastakis, R. J. Schoelkopf, M. H. Devoret, and M. Mirrahimi, *Hardware-Efficient Autonomous Quantum Memory Protection*, Phys. Rev. Lett. **111**, 120501 (2013).
[13] M. Mirrahimi, Z. Leghtas, V. V. Albert, S. Touzard, R. J. Schoelkopf, L. Jiang, and M. H. Devoret, *Dynamically Protected Cat-Qubits: A New Paradigm for Universal Quantum Computation*, New J. Phys. **16**, 045014 (2014).
[14] K. Noh, V. V. Albert, and L. Jiang, *Quantum Capacity Bounds of Gaussian Thermal Loss Channels and Achievable Rates with Gottesman-Kitaev-Preskill Codes*, IEEE Trans. Inf. Theory **65**, 2563 (2019).
[15] K. Fukui, R. N. Alexander, and P. van Loock, *All-Optical Long-Distance Quantum Communication with Gottesman-Kitaev-Preskill Qubits*, Phys. Rev. Res. **3**, 033118 (2021).
[16] W. J. Munro, N. L. Piparo, J. Dias, M. Hanks, and K. Nemoto, *Designing Tomorrow's Quantum Internet*, AVS Quantum Sci. **4**, 020503 (2022).
[17] P. Campagne-Ibarcq *et al.*, *Quantum Error Correction of a Qubit Encoded in Grid States of an Oscillator*, Nature (London) **584**, 368 (2020).
[18] B. de Neeve, T. L. Nguyen, T. Behrle, and J. P. Home, *Error Correction of a Logical Grid State Qubit by Dissipative Pumping*, Nat. Phys. **18**, 296 (2022).
[19] B. C. Travaglione and G. J. Milburn, *Preparing Encoded States in an Oscillator*, Phys. Rev. A **66**, 052322 (2002).
[20] S. Pirandola, S. Mancini, D. Vitali, and P. Tombesi, *Constructing Finite-Dimensional Codes with Optical Continuous Variables*, Europhys. Lett. **68**, 323 (2004).
[21] S. Pirandola, S. Mancini, D. Vitali, and P. Tombesi, *Continuous Variable Encoding by Ponderomotive Interaction*, Eur. Phys. J. D **37**, 283 (2006).
[22] H. M. Vasconcelos, L. Sanz, and S. Glancy, *All-Optical Generation of States for "Encoding a Qubit in an Oscillator"*, Opt. Lett. **35**, 3261 (2010).
[23] C. Flühmann, T. L. Nguyen, M. Marinelli, V. Negnevitsky, K. Mehta, and J. P. Home, *Encoding a Qubit in a Trapped-Ion Mechanical Oscillator*, Nature (London) **566**, 513 (2019).
[24] D. Su, C. R. Myers, and K. K. Sabapathy, *Conversion of Gaussian States to Non-Gaussian States Using Photon-Number-Resolving Detectors*, Phys. Rev. A **100**, 052301 (2019).
[25] M. Eaton, R. Nehra, and O. Pfister, *Non-Gaussian and Gottesman-Kitaev-Preskill State Preparation by Photon Catalysis*, New J. Phys. **21**, 113034 (2019).
[26] I. Tzitrin, J. E. Bourassa, N. C. Menicucci, and K. K. Sabapathy, *Progress towards Practical Qubit Computation Using Approximate Gottesman-Kitaev-Preskill Codes*, Phys. Rev. A **101**, 032315 (2020).

[27] K. Fukui, M. Endo, W. Asavanant, A. Sakaguchi, J. I. Yoshikawa, and A. Furusawa, *Generating the Gottesman-Kitaev-Preskill Qubit Using a Cross-Kerr Interaction between Squeezed Light and Fock States in Optics*, Phys. Rev. A **105**, 022436 (2022).
[28] J. Hastrup and U. L. Andersen, *Protocol for Generating Optical Gottesman-Kitaev-Preskill States with Cavity QED*, Phys. Rev. Lett. **128**, 170503 (2022).
[29] D. T. Le, A. Grimsmo, C. Müller, and T. M. Stace, *Doubly Nonlinear Superconducting Qubit*, Phys. Rev. A **100**, 062321 (2019).
[30] M. Rymarz, S. Bosco, A. Ciani, and D. P. DiVincenzo, *Hardware-Encoding Grid States in a Nonreciprocal Super-Conducting Circuit*, Phys. Rev. X **11**, 011032 (2021).
[31] V. V. Sivak *et al.*, *Real-Time Quantum Error Correction beyond Break-Even*, Nature (London) **616**, 50 (2023).
[32] N. C. Menicucci, *Fault-Tolerant Measurement-Based Quantum Computing with Continuous-Variable Cluster States*, Phys. Rev. Lett. **112**, 120504 (2014).
[33] S. Takeda and A. Furusawa, *Toward Large-Scale Fault-Tolerant Universal Photonic Quantum Computing*, APL Photonics **4**, 060902 (2019).
[34] D. J. Weigand and B. M. Terhal, *Generating Grid States from Schrödinger-Cat States without Postselection*, Phys. Rev. A **97**, 022341 (2018).
[35] U. L. Andersen, T. Gehring, C. Marquardt, and G. Leuchs, *30 Years of Squeezed Light Generation*, Phys. Scr. **91**, 053001 (2016).
[36] A. Eickbusch, V. Sivak, A. Z. Ding, S. S. Elder, S. R. Jha, J. Venkatraman, B. Royer, S. M. Girvin, R. J. Schoelkopf, and M. H. Devoret, *Fast Universal Control of an Oscillator with Weak Dispersive Coupling to a Qubit*, Nat. Phys. **18**, 1464 (2022).
[37] I. Kaminer, M. Mutzafi, A. Levy, G. Harari, H. H. Sheinfux, S. Skirlo, J. Nemirovsky, J. D. Joannopoulos, M. Segev, and M. Soljacic, *Quantum Čerenkov Radiation: Spectral Cutoffs and the Role of Spin and Orbital Angular Momentum*, Phys. Rev. X **6**, 011006 (2016).
[38] E. Rotunno *et al.*, *One-Dimensional Ghost Imaging with an Electron Microscope: A Route Towards Ghost Imaging with Inelastically Scattered Electrons*, arXiv:2106.08955.
[39] G. Guzzinati, A. Béché, H. Lourenço-Martins, J. Martin, M. Kociak, and J. Verbeeck, *Probing the Symmetry of the Potential of Localized Surface Plasmon Resonances with Phase-Shaped Electron Beams*, Nat. Commun. **8**, 14999 (2017).
[40] X. Bendaña, A. Polman, and F. J. García De Abajo, *Single-Photon Generation by Electron Beams*, Nano Lett. **11**, 5099 (2011).
[41] A. Feist *et al.*, *Cavity-Mediated Electron-Photon Pairs*, Science **377**, 777 (2022).
[42] A. Ben Hayun, O. Reinhardt, J. Nemirovsky, A. Karnieli, N. Rivera, and I. Kaminer, *Shaping Quantum Photonic States Using Free Electrons*, Sci. Adv. **7**, 4270 (2021).
[43] V. di Giulio, O. Kfir, C. Ropers, and F. J. García De Abajo, *Modulation of Cathodoluminescence Emission by Interference with External Light*, ACS Nano **15**, 7290 (2021).
[44] F. J. García De Abajo and V. di Giulio, *Optical Excitations with Electron Beams: Challenges and Opportunities*, ACS Photonics **8**, 945 (2021).
[45] A. Karnieli, N. Rivera, A. Arie, and I. Kaminer, *The Coherence of Light Is Fundamentally Tied to the Quantum Coherence of the Emitting Particle*, Sci. Adv. **7**, 8096 (2021).
[46] O. Kfir, V. di Giulio, F. Javier García de Abajo, and C. Ropers, *Optical Coherence Transfer Mediated by Free Electrons*, Sci. Adv. **7**, 6380 (2021).
[47] B. Barwick, D. J. Flannigan, and A. H. Zewail, *Photon-Induced Near-Field Electron Microscopy*, Nature (London) **462**, 902 (2009).
[48] A. Feist, K. E. Echternkamp, J. Schauss, S. V. Yalunin, S. Schäfer, and C. Ropers, *Quantum Coherent Optical Phase Modulation in an Ultrafast Transmission Electron Microscope*, Nature (London) **521**, 200 (2015).
[49] K. E. Priebe, C. Rathje, S. V. Yalunin, T. Hohage, A. Feist, S. Schäfer, and C. Ropers, *Attosecond Electron Pulse Trains and Quantum State Reconstruction in Ultrafast Transmission Electron Microscopy*, Nat. Photonics **11**, 793 (2017).
[50] K. Wang, R. Dahan, M. Shentcis, Y. Kauffmann, A. Ben Hayun, O. Reinhardt, S. Tsesses, and I. kaminer, *Coherent Interaction between Free Electrons and a Photonic Cavity*, Nature (London) **582**, 50 (2020).
[51] G. M. Vanacore, I. Madan, and F. Carbone, *Spatio-Temporal Shaping of a Free-Electron Wave Function via Coherent Light–Electron Interaction*, Riv. del Nuovo Cim. **43**, 567 (2020).
[52] I. Madan, G. M. Vanacore, S. Gargiulo, T. LaGrange, and F. Carbone, *The Quantum Future of Microscopy: Wave Function Engineering of Electrons, Ions, and Nuclei*, Appl. Phys. Lett. **116**, 230502 (2020).
[53] M. Uchida and A. Tonomura, *Generation of Electron Beams Carrying Orbital Angular Momentum*, Nature (London) **464**, 737 (2010).
[54] J. Verbeeck, H. Tian, and P. Schattschneider, *Production and Application of Electron Vortex Beams*, Nature (London) **467**, 301 (2010).
[55] B. J. McMorran, A. Agrawal, I. M. Anderson, A. A. Herzing, H. J. Lezec, J. J. McClelland, and J. Unguris, *Electron Vortex Beams with High Quanta of Orbital Angular Momentum*, Science **331**, 192 (2011).
[56] N. Voloch-Bloch, Y. Lereah, Y. Lilach, A. Gover, and A. Arie, *Generation of Electron Airy Beams*, Nature (London) **494**, 331 (2013).
[57] R. Shiloh, Y. Lereah, Y. Lilach, and A. Arie, *Sculpturing the Electron Wave Function Using Nanoscale Phase Masks*, Ultramicroscopy **144**, 26 (2014).
[58] V. Grillo, E. Karimi, G. C. Gazzadi, S. Frabboni, M. R. Dennis, and R. W. Boyd, *Generation of Nondiffracting Electron Bessel Beams*, Phys. Rev. X **4**, 011013 (2014).
[59] J. Verbeeck, A. Béché, K. Müller-Caspary, G. Guzzinati, M. A. Luong, and M. den Hertog, *Demonstration of a* 2×2 *Programmable Phase Plate for Electrons*, Ultramicroscopy **190**, 58 (2018).
[60] J. Verbeeck and A. Béché, *Spatial Phase Manipulation of Charged Particle Beam*, U.S. Patent No. US11062872B2

(2021) [https://patents.google.com/patent/US11062872B2/en].

[61] G. M. Vanacore *et al.*, *Attosecond Coherent Control of Free-Electron Wave Functions Using Semi-Infinite Light Fields*, Nat. Commun. **9**, 2694 (2018).

[62] A. H. Tavabi *et al.*, *Experimental Demonstration of an Electrostatic Orbital Angular Momentum Sorter for Electron Beams*, Phys. Rev. Lett. **126**, 094802 (2021).

[63] S. Tsesses, R. Dahan, K. Wang, T. Bucher, K. Cohen, O. Reinhardt, G. Bartal, and I. Kaminer, *Tunable Photon-Induced Spatial Modulation of Free Electrons*, Nat. Mater. **22**, 345 (2023).

[64] O. Kfir, H. Lourenço-Martins, G. Storeck, M. Sivis, T. R. Harvey, T. J. Kippenberg, A. Feist, and C. Ropers, *Controlling Free Electrons with Optical Whispering-Gallery Modes*, Nature (London) **582**, 46 (2020).

[65] R. Dahan *et al.*, *Resonant Phase-Matching between a Light Wave and a Free-Electron Wavefunction*, Nat. Phys. **16**, 1123 (2020).

[66] Y. Adiv *et al.*, *Quantum Nature of Dielectric Laser Accelerators*, Phys. Rev. X **11**, 041042 (2021).

[67] A. Polman, M. Kociak, and F. J. García De Abajo, *Electron-Beam Spectroscopy for Nanophotonics*, Nat. Mater. **18**, 1158 (2019).

[68] C. Roques-Carmes, S. E. Kooi, Y. Yang, N. Rivera, P. D. Keathley, J. D. Joannopoulos, S. G. Johnson, I. Kaminer, K. K. Berggren, and M. Soljačić, *Free-Electron-Light Interactions in Nanophotonics*, Appl. Phys. Rev. **10**, 011303 (2023).

[69] M. V. Tsarev, A. Ryabov, and P. Baum, *Free-Electron Qubits and Maximum-Contrast Attosecond Pulses via Temporal Talbot Revivals*, Phys. Rev. Res. **3**, 043033 (2021).

[70] R. Dahan *et al.*, *Imprinting the Quantum Statistics of Photons on Free Electrons*, Science **373**, 7128 (2021).

[71] J. W. Henke *et al.*, *Integrated Photonics Enables Continuous-Beam Electron Phase Modulation*, Nature (London) **600**, 653 (2021).

[72] R. Shiloh, T. Chlouba, and P. Hommelhoff, *Quantum-Coherent Light-Electron Interaction in a Scanning Electron Microscope*, Phys. Rev. Lett. **128**, 235301 (2022).

[73] F. J. Garcia De Abajo, A. Asenjo-Garcia, and M. Kociak, *Multiphoton Absorption and Emission by Interaction of Swift Electrons with Evanescent Light Fields*, Nano Lett. **10**, 1859 (2010).

[74] S. T. Park, M. Lin, and A. H. Zewail, *Photon-Induced Near-Field Electron Microscopy (PINEM): Theoretical and Experimental*, New J. Phys. **12**, 123028 (2010).

[75] O. Reinhardt and I. Kaminer, *Theory of Shaping Electron Wavepackets with Light*, ACS Photonics **7**, 2859 (2020).

[76] S. V. Yalunin, A. Feist, and C. Ropers, *Tailored High-Contrast Attosecond Electron Pulses for Coherent Excitation and Scattering*, Phys. Rev. Res. **3**, L032036 (2021).

[77] N. Varkentina *et al.*, *Cathodoluminescence Excitation Spectroscopy: Nanoscale Imaging of Excitation Pathways*, Sci. Adv. **8**, 4947 (2022).

[78] O. Kfir, *Entanglements of Electrons and Cavity Photons in the Strong-Coupling Regime*, Phys. Rev. Lett. **123**, 103602 (2019).

[79] V. di Giulio, M. Kociak, and F. J. G. de Abajo, *Probing Quantum Optical Excitations with Fast Electrons*, Optica **6**, 1524 (2019).

[80] V. V. Albert, J. P. Covey, and J. Preskill, *Robust Encoding of a Qubit in a Molecule*, Phys. Rev. X **10**, 031050 (2020).

[81] F. J. García de Abajo, *Optical Excitations in Electron Microscopy*, Rev. Mod. Phys. **82**, 209 (2010).

[82] P. Baum and A. H. Zewail, *Attosecond Electron Pulses for 4D Diffraction and Microscopy*, Proc. Natl. Acad. Sci. U.S.A. **104**, 18409 (2007).

[83] M. Kozák, T. Eckstein, N. Schönenberger, and P. Hommelhoff, *Inelastic Ponderomotive Scattering of Electrons at a High-Intensity Optical Travelling Wave in Vacuum*, Nat. Phys. **14**, 121 (2018).

[84] N. Talebi and C. Lienau, *Interference between Quantum Paths in Coherent Kapitza-Dirac Effect*, New J. Phys. **21**, 093016 (2019).

[85] See Supplemental Material at http://link.aps.org/supplemental/10.1103/PhysRevX.13.031001, which includes the formulation for generating cat and GKP states using free electrons, along with detailed calculations regarding the probability and fidelity of postselecting these states.

[86] V. V. Albert *et al.*, *Performance and Structure of Single-Mode Bosonic Codes*, Phys. Rev. A **97**, 032346 (2018).

[87] A. L. Grimsmo and S. Puri, *Quantum Error Correction with the Gottesman-Kitaev-Preskill Code*, PRX Quantum **2**, 020101 (2021).

[88] K. Fukui, A. Tomita, A. Okamoto, and K. Fujii, *High-Threshold Fault-Tolerant Quantum Computation with Analog Quantum Error Correction*, Phys. Rev. X **8**, 021054 (2018).

[89] J. E. Bourassa *et al.*, *Blueprint for a Scalable Photonic Fault-Tolerant Quantum Computer*, Quantum **5**, 392 (2021).

[90] S. Bravyi and A. Kitaev, *Universal Quantum Computation with Ideal Clifford Gates and Noisy Ancillas*, Phys. Rev. A **71**, 022316 (2005).

[91] B. Q. Baragiola, G. Pantaleoni, R. N. Alexander, A. Karanjai, and N. C. Menicucci, *All-Gaussian Universality and Fault Tolerance with the Gottesman-Kitaev-Preskill Code*, Phys. Rev. Lett. **123**, 200502 (2019).

[92] G. Baranes, R. Ruimy, A. Gorlach, and I. Kaminer, *Free Electrons Can Induce Entanglement between Photons*, npj Quantum Inf. **8**, 32 (2022).

[93] S. Bravyi, D. Gosset, and R. König, *Quantum Advantage with Shallow Circuits*, Science **362**, 308 (2018).

[94] S. Bravyi, D. Gosset, R. König, and M. Tomamichel, *Quantum Advantage with Noisy Shallow Circuits*, Nat. Phys. **16**, 1040 (2020).

[95] W. Krakow and L. A. Howland, *Multiplexing Electron Beam Patterns Using Single-Crystal Thin Films*, J. Phys. E **12**, 984 (1979).

[96] P. C. Post, A. Mohammadi-Gheidari, C. W. Hagen, and P. Kruit, *Parallel Electron-Beam-Induced Deposition Using a Multi-Beam Scanning Electron Microscope*, J. Vac. Sci. Technol. B **29**, 06F310 (2011).

[97] M. Esashi, A. Kojima, N. Ikegami, H. Miyaguchi, and N. Koshida, *Development of Massively Parallel Electron Beam Direct Write Lithography Using Active-Matrix*

Nanocrystalline-Silicon Electron Emitter Arrays, Microsyst. Nanoeng. **1**, 15029 (2015).
[98] A. E. Turner, C. W. Johnson, P. Kruit, and B. J. McMorran, *Interaction-Free Measurement with Electrons*, Phys. Rev. Lett. **127**, 110401 (2021).
[99] H. Bombin, I. H. Kim, D. Litinski, N. Nickerson, M. Pant, F. Pastawski, S. Roberts, and T. Rudolph, *Interleaving: Modular Architectures for Fault-Tolerant Photonic Quantum Computing*, arXiv:2103.08612.
[100] S. Uhlemann, H. Müller, J. Zach, and M. Haider, *Thermal Magnetic Field Noise: Electron Optics and Decoherence*, Ultramicroscopy **151**, 199 (2015).
[101] A. Howie, *Mechanisms of Decoherence in Electron Microscopy*, Ultramicroscopy **111**, 761 (2011).
[102] G. Huang, N. J. Engelsen, O. Kfir, C. Ropers, and T. J. Kippenberg, *Quantum State Heralding Using Photonic Integrated Circuits with Free Electrons*, arXiv:2206.08098.
[103] C. W. Barlow Myers, N. J. Pine, and W. A. Bryan, *Femtosecond Transmission Electron Microscopy for Nanoscale Photonics: A Numerical Study*, Nanoscale **10**, 20628 (2018).
[104] M. Yannai, Y. Adiv, R. Dahan, A. Gorlach, N. Rivera, K. Wang, and I. Kaminer, *Lossless Electron Beam Monochromator in an Ultrafast TEM Using Near-field THz Radiation*, in *Proceedings of the Conference on Lasers and Electro-Optics, P. STu4L.2.* (Optica Publishing Group, Washington, DC, 2022), 10.1364/CLEO_SI.2022.STu4L.2.
[105] Y. Adiv *et al.*, *Observation of 2D Cherenkov Radiation*, Phys. Rev. X **13**, 011002 (2023).
[106] A. R. Faruqi and G. McMullan, *Direct Imaging Detectors for Electron Microscopy*, Nucl. Instrum. Methods Phys. Res., Sect. A **878**, 180 (2018).
[107] K. A. Paton, M. C. Veale, X. Mu, C. S. Allen, D. Maneuski, C. Kübel, V. O'Shea, A. I. Kirkland, and D. McGrouther, *Quantifying the Performance of a Hybrid Pixel Detector with GaAs:Cr Sensor for Transmission Electron Microscopy*, Ultramicroscopy **227**, 113298 (2021).
[108] Y. Yang, C. Roques-Carmes, S. E. Kooi, H. Tang, J. Beroz, E. Mazur, I. Kaminer, J. D. Joannopoulos, and M. Soljačić, *Photonic Flatband Resonances for Free-Electron Radiation*, Nature (London) **613**, 42 (2021).
[109] S. Molesky, Z. Lin, A. Y. Piggott, W. Jin, J. Vucković, and A. W. Rodriguez, *Inverse Design in Nanophotonics*, Nat. Photonics **12**, 659 (2018).
[110] F. Hasselbach, *Progress in Electron- and Ion-Interferometry*, Rep. Prog. Phys. **73**, 016101 (2010).
[111] M. Tsarev, A. Ryabov, and P. Baum, *Measurement of Temporal Coherence of Free Electrons by Time-Domain Electron Interferometry*, Phys. Rev. Lett. **127**, 165501 (2021).
[112] I. Tzitrin, T. Matsuura, R. N. Alexander, G. Dauphinais, J. E. Bourassa, K. K. Sabapathy, N. C. Menicucci, and I. Dhand, *Fault-Tolerant Quantum Computation with Static Linear Optics*, PRX Quantum **2**, 040353 (2021).
[113] D. Jannis, K. Müller-Caspary, A. Béché, A. Oelsner, and J. Verbeeck, *Spectroscopic Coincidence Experiments in Transmission Electron Microscopy*, Appl. Phys. Lett. **114**, 143101 (2019).
[114] C. Roques-Carmes, N. Rivera, J. D. Joannopoulos, M. Soljačić, and I. Kaminer, *Nonperturbative Quantum Electrodynamics in the Cherenkov Effect*, Phys. Rev. X **8**, 041013 (2018).
[115] O. Reinhardt, C. Mechel, M. Lynch, and I. Kaminer, *Free-Electron Qubits*, Ann. Phys. (Amsterdam) **533**, 2000254 (2021).
[116] N. Fabre *et al.*, *Generation of a Time-Frequency Grid State with Integrated Biphoton Frequency Combs*, Phys. Rev. A **102**, 012607 (2020).
[117] A. Sørensen and K. Mølmer, *Entanglement and Quantum Computation with Ions in Thermal Motion*, Phys. Rev. A **62**, 022311 (2000).
[118] P. C. Haljan, K. A. Brickman, L. Deslauriers, P. J. Lee, and C. Monroe, *Spin-Dependent Forces on Trapped Ions for Phase-Stable Quantum Gates and Entangled States of Spin and Motion*, Phys. Rev. Lett. **94**, 153602 (2005).
[119] M. Boissonneault, J. M. Gambetta, and A. Blais, *Dispersive Regime of Circuit QED: Photon-Dependent Qubit Dephasing and Relaxation Rates*, Phys. Rev. A **79**, 013819 (2009).